

# Heavy-light decay topologies as a new strategy to discover a heavy gluon

Cesare Bini<sup>a</sup>, Roberto Contino<sup>a</sup>, Natascia Vignaroli<sup>a,b</sup>

<sup>a</sup> *Dipartimento di Fisica, Sapienza Università di Roma and INFN, Italy*

<sup>b</sup> *Department of Physics and Astronomy, Iowa State University, Ames, IA 50011*

## Abstract

We study the collider phenomenology of the lightest Kaluza-Klein excitation of the gluon,  $G^*$ , in theories with a warped extra dimension. We do so by means of a two-site effective lagrangian which includes only the lowest-lying spin-1 and spin-1/2 resonances. We point out the importance of the decays of  $G^*$  to one SM plus one heavy fermion, that were overlooked in the previous literature. It turns out that, when kinematically allowed, such heavy-light decays are powerful channels for discovering the  $G^*$ . In particular, we present a parton-level Montecarlo analysis of the final state  $Wtb$  that follows from the decay of  $G^*$  to one SM top or bottom quark plus its heavy partner. We find that at  $\sqrt{s} = 7 \text{ TeV}$  and with  $10 \text{ fb}^{-1}$  of integrated luminosity, the LHC can discover a KK gluon with mass in the range  $M_{G^*} = (1.8 - 2.2) \text{ TeV}$  if its coupling to a pair of light quarks is  $g_{G^*q\bar{q}} = (0.2 - 0.5)g_3$ . The same process is also competitive for the discovery of the top and bottom partners as well. We find, for example, that the LHC at  $\sqrt{s} = 7 \text{ TeV}$  can discover a 1 TeV KK bottom quark with an integrated luminosity of  $(5.3 - 0.61) \text{ fb}^{-1}$  for  $g_{G^*q\bar{q}} = (0.2 - 0.5)g_3$ .

# 1 Introduction

One of the robust predictions of theories with a warped extra-dimension [1] and fields propagating in the bulk [2–4] is the existence of heavier copies of the gluon with  $\sim \text{TeV}$  mass, its Kaluza-Klein (KK) excitations. The phenomenology of the lightest of the KK gluons, which we will denote as  $G^*$ , has been extensively studied [5–10]. In the theoretically attractive framework where the hierarchy of masses and mixings of the Standard Model (SM) quarks follows from the geography of wave functions in the bulk, while the 5D Yukawa couplings are flavor anarchic [3, 4, 11], the couplings of the heavy gluon  $G^*$  to the SM quarks are dictated by an inverse hierarchy, where the largest coupling is to the top quark. In this case the decay rate of  $G^*$  to pairs of top quarks is typically large and dominates over the decay rate to two light quarks.

Experiments at the Tevatron and the LHC have been testing this theoretical picture performing several searches for the heavy gluon  $G^*$  in dijet final states [12, 13] and in the  $t\bar{t}$  channel [14–19].<sup>1</sup> In the latter case, some analyses do not attempt to reconstruct the top quarks, and are in fact searches for  $WbWb$  resonances. Others instead look for highly boosted top quarks and make use of dedicated top-tagging techniques to reduce the SM background, following the original suggestion of Refs. [5, 6]. Taken all together, these experimental results impose important constraints on the value of the mass and couplings of the heavy gluon, and in turn on the parameter space of the extra-dimensional theories.

In addition to the KK gluon, new heavy fermions are also naturally predicted in theories with a warped extra dimension as the Kaluza-Klein excitations of the SM quarks and leptons. In particular, in models where the Higgs doublet is a pseudo Nambu-Goldstone boson of a larger symmetry breaking [20, 21], the lightest KK top regulates the quadratically divergent contribution of the SM top quark to the Higgs mass term. By naturalness arguments, it is thus expected to have a mass below  $\sim 1 \text{ TeV}$ . The coupling of  $G^*$  to the heavy fermions is typically large, so that, if kinematically allowed, the heavy gluon decays to a pair of heavy fermions with a large rate. In this limit the total decay width of  $G^*$  becomes very large, due both to the large value of the couplings and to the multiplicity of available decay channels, making its discovery quite challenging [22].

On the other hand,  $G^*$  can also decay to one SM plus one heavy fermion. Specifically, the most important channels in scenarios with flavor anarchy are those with one SM top or bottom quark plus its heavy copy. If the threshold to two heavy fermions is kinematically closed, the branching ratio of these heavy-light channels can be large in a wide portion of the parameter space. At the same time the branching ratio to pairs of SM quarks is reduced, making the standard analyses of dijet and  $t\bar{t}$  final states less constraining. The importance of the heavy-light decays at the Tevatron was already pointed out in Ref. [23] in the context of a different theoretical framework. No detailed study however has been done so far, to our knowledge, to assess the prospects of observing the heavy-light decays of  $G^*$  at the LHC.

In this paper we present a first analysis of this kind and outline a simple cut-based strategy to maximize the signal significance over the SM background. Some preliminary results have already been presented in Ref. [24]. We find that, thanks to their distinct topology, decays to one SM plus one heavy fermion are extremely clean channels with a strong potential for

---

<sup>1</sup>Here we list only those experimental searches that presently impose the strongest bounds, omitting previous or less constraining analyses.

the discovery not just of  $G^*$ , but of the KK top and bottom as well. Our analysis suggests that the discovery reach on these latter can be larger than the one obtained by exploiting the more studied processes of QCD pair production [25, 22, 26–28] and electroweak single production [29–32].

Although our study is performed in the specific context of warped extra-dimensional theories, we believe that our results apply to a broader class of models beyond the SM where both a heavy spin-1 color-octet and heavy top or bottom fermions exist, like for example the top-quark seesaw model [33, 34].

The paper is organized as follows. In Section 2 we define the effective two-site model that we adopt to study the phenomenology of the heavy gluon and heavy fermions. We derive the  $G^*$  production cross section and the relevant decay rates, showing that the branching ratio of  $G^*$  to one SM plus one heavy fermion is large when kinematically allowed. In Section 3 we study the prospects of observing the heavy-light decays of  $G^*$  in  $Wtb$  events at the LHC. We perform a Montecarlo simulation of the signal and the main SM backgrounds and design a simple set of kinematic cuts that maximizes the discovery significance. In Section 4 we discuss the results obtained and draw our conclusions. Finally, Appendix A contains a few results used in discussing the effective model, while details on how the statistical errors are computed are given in Appendix B.

## 2 An effective theory of the heavy gluon and the top partners

Instead of considering the full set of particles and interactions arising in a specific model, we will work in the framework of an effective theory that includes only the lowest-lying resonances and reproduces, in the same spirit of chiral lagrangians in QCD, the low-energy limit of a large set of warped extra-dimensional theories with a custodial symmetry in the bulk [35]. Specifically, we will construct the effective lagrangian by following the rules of deconstruction defined in Ref. [36], and adopt the ‘dual’ language of strongly-interacting dynamics to describe the theory [37, 38]. In this perspective, the new heavy particles arise as composite states of a new strong sector, which are coupled to the SM elementary ones via linear mixing terms, leading to a scenario of partial compositeness [39, 36]. The Higgs is also a bound state of the new dynamics and has direct couplings only to the composite fermions.

### 2.1 The model

We consider the case in which the composite sector has an  $SU(3)_c \times O(4) \times U(1)_X$  global symmetry, with  $O(4) \supset SO(4) \sim SU(2)_L \times SU(2)_R$ , where  $O(4)$  contains a discrete parity  $P_{LR}$  under which  $SU(2)_L$  and  $SU(2)_R$  are exchanged. The two building blocks of the model are the elementary sector and the composite sector. The particle content of the elementary sector is that of the SM without the Higgs, and the  $SU(3)_c \times SU(2)_L \times U(1)_Y$  elementary fields gauge the corresponding global invariance of the strong dynamics, with  $Y = T_R^3 + X$ . The composite sector comprises a heavy gluon,  $G^*$ , which transforms as  $(\mathbf{8}, \mathbf{1}, \mathbf{1})_0$  under

$SU(3)_c \times SU(2)_L \times SU(2)_R \times U(1)_X$ , the composite Higgs

$$\mathcal{H} = (\mathbf{1}, \mathbf{2}, \mathbf{2})_0 = \begin{bmatrix} \phi_0^\dagger & \phi^+ \\ -\phi^- & \phi_0 \end{bmatrix}, \quad (1)$$

and the following set of vector-like composite fermions:

$$\begin{aligned} \mathcal{Q} &= (\mathbf{3}, \mathbf{2}, \mathbf{2})_{2/3} = \begin{bmatrix} T & T_{5/3} \\ B & T_{2/3} \end{bmatrix}, & \tilde{T} &= (\mathbf{3}, \mathbf{1}, \mathbf{1})_{2/3}, \\ \mathcal{Q}' &= (\mathbf{3}, \mathbf{2}, \mathbf{2})'_{-1/3} = \begin{bmatrix} B_{-1/3} & T' \\ B_{-4/3} & B' \end{bmatrix}, & \tilde{B} &= (\mathbf{3}, \mathbf{1}, \mathbf{1})_{-1/3}. \end{aligned} \quad (2)$$

Other composite states, for example spin-1 resonances with electroweak quantum numbers, are in general present in the spectrum of realistic models, but will not be considered here for simplicity. The quantum numbers of the composite fermions and the Higgs under  $SU(3)_c \times SU(2)_L \times SU(2)_R \times U(1)_X$  are those specified in eqs.(1),(2). The fermions, in particular, can be arranged in two fundamentals of  $SO(5)$ , and in fact our effective model describes the low-energy regime of the  $SO(5)/SO(4)$  theories introduced in Refs. [40, 41], in the limit in which only the leading terms in an expansion in powers of the Higgs field are retained (see Refs. [42, 43], for two- and three-site effective theories where the full Higgs non-linearities are included). For this reason, we will dub our two-site model as TS5. As it will be even more evident shortly, it extends the two-site model of Ref. [27] to include the heavy gluon and the composite fermions needed to give mass to the bottom quark.

The lagrangian that describes our effective theory is the following (we work in the electroweak gauge-less limit, and omit the terms involving the  $SU(2)_L \times U(1)_Y$  elementary gauge fields, which play no role in our analysis):

$$\mathcal{L} = \mathcal{L}_{elementary} + \mathcal{L}_{composite} + \mathcal{L}_{mixing} \quad (3)$$

$$\mathcal{L}_{elementary} = -\frac{1}{4g_{el3}^2} G_{\mu\nu} G^{\mu\nu} + \bar{q}_L^i i \not{D} q_L^i + \bar{u}_R^i i \not{D} u_R^i + \bar{d}_R^i i \not{D} d_R^i \quad (4)$$

$$\begin{aligned} \mathcal{L}_{composite} &= -\frac{1}{4g_{*3}^2} G_{\mu\nu}^* G^{*\mu\nu} + \frac{1}{2} \text{Tr} \{ \partial_\mu \mathcal{H}^\dagger \partial^\mu \mathcal{H} \} - V(\mathcal{H}^\dagger \mathcal{H}) \\ &+ \text{Tr} \{ \bar{\mathcal{Q}} (i \not{\partial} - \mathcal{G}^* - \bar{m}_{\mathcal{Q}}) \mathcal{Q} \} + \bar{\tilde{T}} (i \not{\partial} - \mathcal{G}^* - \bar{m}_{\tilde{T}}) \tilde{T} \\ &+ \text{Tr} \{ \bar{\mathcal{Q}}' (i \not{\partial} - \mathcal{G}^* - \bar{m}_{\mathcal{Q}'}) \mathcal{Q}' \} + \bar{\tilde{B}} (i \not{\partial} - \mathcal{G}^* - \bar{m}_{\tilde{B}}) \tilde{B} \\ &- Y_{*U} \text{Tr} \{ \bar{\mathcal{Q}} \mathcal{H} \} \tilde{T} - Y_{*D} \text{Tr} \{ \bar{\mathcal{Q}}' \mathcal{H} \} \tilde{B} + h.c. \end{aligned} \quad (5)$$

$$\begin{aligned} \mathcal{L}_{mixing} &= \frac{1}{2} \frac{\bar{M}_{G^*}^2}{g_{*3}^2} (G_\mu - G_\mu^*)^2 - \Delta_{L1} \bar{q}_L^3 (T, B) - \Delta_{L2} \bar{q}_L^3 (T', B') \\ &- \Delta_{tR} \bar{t}_R \tilde{T} - \Delta_{bR} \bar{b}_R \tilde{B} + h.c., \end{aligned} \quad (6)$$

where  $V(\mathcal{H}^\dagger\mathcal{H})$  is the Higgs potential, and the derivative  $D_\mu$  is covariant under  $SU(3)_c$  transformations. The superscript  $i$  in eq.(4) runs over the three SM families ( $i = 1, 2, 3$ ), with  $q_L^3 \equiv (t_L, b_L)$ ,  $u_R^3 \equiv t_R$ ,  $d_R^3 \equiv b_R$ . In addition to the Higgs mass and the self-couplings contained in the Higgs potential, the lagrangian (3) has thirteen free parameters: four composite masses in the fermionic sector ( $\bar{m}_Q, \bar{m}_{Q'}, \bar{m}_{\tilde{T}}, \bar{m}_{\tilde{B}}$ ); one for  $G^*$  ( $M_{G^*}$ ); four mass mixing terms ( $\Delta_{L1}, \Delta_{L2}, \Delta_{tR}, \Delta_{bR}$ ); two composite Yukawa couplings ( $Y_{*U}, Y_{*D}$ ); and two gauge couplings ( $g_{el3}, g_{*3}$ ).

By construction, the elementary fields couple to the composite ones only through the mass mixing lagrangian  $\mathcal{L}_{mixing}$ . This implies that the SM Yukawa couplings arise only through the couplings of the Higgs to the composite fermions, and their mixings to the elementary fermions. We consider the case in which the strong sector is flavor anarchic [3, 4, 11]. Under this assumption the hierarchy in the masses and mixings of the SM quarks follows from the hierarchy in the composite/elementary mixing parameters. Reproducing the full spectrum of quark masses and the Cabibbo-Kobayashi-Maskawa matrix requires introducing in the lagrangian three families of heavy fermions and three sets of mixing terms with coefficients  $\{\Delta_{L1}^i, \Delta_{L2}^i, \Delta_{uR}^i, \Delta_{dR}^i\}$ , one for each SM flavor  $i$ . In this case, on the other hand, the mixing parameters of the light elementary quarks are small and their effect can be neglected in studying the  $G^*$  phenomenology, so that one can focus on just the third generation of composite fermions.<sup>2</sup> These two simplifications have in fact been applied in writing eqs.(5),(6), and are justified a posteriori by our assumption of flavor anarchy in the strong sector.<sup>3</sup> The ‘anarchic’ scenario has been extensively studied in the framework of 5D warped models, see Refs. [44–49]. Although flavor-changing neutral effects are parametrically suppressed by the degree of compositeness of the SM fermions, a mechanism which has been dubbed RS-GIM flavor protection [45], it has been shown that numerically strong bounds on the masses of the KK gluon and of the KK fermions still generically follow from CP-violating observables in the kaon sector, namely  $\epsilon_K$  [46,47] and  $\epsilon'/\epsilon$  [49], the neutron electric dipole moment [45], and  $b \rightarrow s\gamma$  [48]. Several solutions have been proposed to evade these bounds, without renouncing to the explanation of the SM flavor hierarchy, in which the strong sector (*i.e.* the bulk of 5D models) is assumed to be invariant under additional flavor symmetries [50–53] or to preserve CP [10]. In these scenarios the KK gluon can have a mass as light as a few TeVs and its phenomenology is not qualitatively modified. In the following we will assume that some mechanism is at work to alleviate the flavor bounds and we will estimate the LHC reach on the heavy masses without imposing any restriction on them.

We assume  $\Delta_{L2} \ll \Delta_{L1}$ , which can naturally follow, for example, from the RG flow in the full theory [40]. In this limit, up to small  $O(\Delta_{L2})$  effects, the  $P_{LR}$  parity of the strong sector is not broken by the coupling of the elementary  $b_L$  to the latter, and the vertex  $Zb\bar{b}$

---

<sup>2</sup>In fact, once produced, heavy fermions of the first two generations will also decay mostly to tops and bottoms, since flavor-changing transitions are not suppressed in the strong sector, while the couplings to the light SM quarks are extremely small, see the discussion in Ref. [36]. In this sense, the addition of the first two generations of heavy fermions in the lagrangian (3) would not qualitatively alter the phenomenology described in this paper.

<sup>3</sup>If the strong sector is not anarchic, the phenomenology can change significantly and additional signatures, like for example the unsuppressed decay of  $G^*$  to light quarks, can appear, see for example Ref. [10]. Our analysis, on the other hand, can still be relevant although the decay modes considered here might not be the dominant ones.

is protected by large tree-level corrections [54].<sup>4</sup> In fact, this protection was the main motivation to require the strong sector to be invariant under  $P_{LR}$  and choose the fermionic representations of eq.(2). We further require  $\Delta_{tR} \sim \Delta_{bR}$ , so that the small ratio  $m_b/m_t$  follows from the hierarchy  $\Delta_{L2}/\Delta_{L1} \ll 1$ . Notice also that for  $\Delta_{L2} \rightarrow 0$  the two-site model of Ref. [27] is contained as a subsector of the TS5 model.

In order to diagonalize the two-site lagrangian (3) one has to make a field rotation from the elementary/composite basis to the mass eigenstate basis [36]. The only exception is given by the first two generations of elementary quarks, since they do not mix with the composite fermions and can thus be directly identified with the corresponding SM states. We performed the field rotation analytically before EWSB by treating  $\Delta_{L2}$  as a small parameter and including only the leading order terms in the perturbative expansion. The final lagrangian is shown in eqs.(27)-(30) of Appendix A. We use an economical notation where symbols denoting elementary (composite) fields before the rotation now indicate the SM (heavy) fields. More details will be reported in a separate publication [56]. Here we just list the relevant parameters that control the spectrum and the interactions of the mass eigenstates and discuss the numerical assumptions we made on them. The elementary/composite rotation in the fermionic sector can be parametrized in terms of six mixing angles, which can be conveniently defined as follows:

$$\tan \varphi_{tR} = \frac{\Delta_{tR}}{\bar{m}_{\bar{T}}}, \quad \tan \varphi_{bR} = \frac{\Delta_{bR}}{\bar{m}_{\bar{B}}}, \quad \tan \varphi_L = \frac{\Delta_{L1}}{\bar{m}_Q}, \quad s_2 = \frac{\Delta_{L2}}{\bar{m}_Q} \cos \varphi_L, \quad (7)$$

plus the two mixing parameters defined in eq.(31) of Appendix A. Here  $\sin \varphi_{tR}$ ,  $\sin \varphi_{bR}$ ,  $\sin \varphi_L$  respectively denote the degree of compositeness of  $t_R$ ,  $b_R$  and  $(t_L, b_L)$ . In the gauge sector, the elementary and the composite couplings  $g_{el3}$ ,  $g_{*3}$  determine the rotation angle  $\theta_3$  and the SM gauge coupling  $g_3$  as follows:

$$\tan \theta_3 = \frac{g_{el3}}{g_{*3}}, \quad g_3 = g_{el3} \cos \theta_3 = g_{*3} \sin \theta_3. \quad (8)$$

The physical masses are given by

$$m_{\bar{T}} = \frac{\bar{m}_{\bar{T}}}{\cos \varphi_{tR}}, \quad m_{\bar{B}} = \frac{\bar{m}_{\bar{B}}}{\cos \varphi_{bR}}, \quad m_T = m_B = \frac{\bar{m}_Q}{\cos \varphi_L}, \quad m_{T'} = m_{B'} \simeq \bar{m}_{Q'}, \quad (9)$$

$$m_{T_{5/3}} = m_{T_{2/3}} = m_T \cos \varphi_L, \quad m_{B_{-4/3}} = m_{B_{-1/3}} = m_{T'}, \quad (10)$$

where only the first four are independent, and

$$M_{G^*} = \frac{\bar{M}_{G^*}}{\cos \theta_3}. \quad (11)$$

There are thus thirteen independent angles and physical masses (in addition to the Higgs mass and self-couplings), corresponding to the initial number of parameters of the lagrangian (3).

---

<sup>4</sup>It has been also pointed out in Ref. [55] that in the case of  $SO(5)/SO(4)$  theories the  $P_{LR}$  parity is accidental at low energy if the fermions transform as fundamental representations of  $SO(5)$ . This ensures automatic protection to  $Zb\bar{b}$  even if the strong dynamics is not  $P_{LR}$  invariant at the fundamental level.

After the EWSB, the SM top and bottom quarks acquire a mass, and the heavy masses in eqs.(9), (10) get corrections of order  $(vY_*/\bar{m})^2$ , where  $v = 246$  GeV is the electroweak scale. In the following, we assume  $r \equiv (vY_*/\bar{m}) \ll 1$  and compute all quantities at leading order in  $r$ .<sup>5</sup> This is in fact a required condition in order to consistently neglect operators with a higher number of Higgs fields in the two-site effective lagrangian. We thus work under the hypothesis of parametrically small  $r$ , although in some of the benchmark points that we will consider  $r$  is numerically not very small.<sup>6</sup> In those cases we expect that our phenomenological analysis still gives an accurate description at the qualitative level, although our formulas can receive quantitatively important corrections. At leading order in  $r$ , the masses of the SM top and bottom quarks read

$$m_t = \frac{v}{\sqrt{2}}Y_{*U} \sin \varphi_L \sin \varphi_{tR}, \quad m_b = \frac{v}{\sqrt{2}}Y_{*D}s_2 \sin \varphi_{bR}. \quad (12)$$

Fixing  $m_t$ ,  $m_b$  and  $g_3$  to their experimental values gives three conditions on the set of parameters. As a further simplification, in what follows we will set

$$Y_{*U} = Y_{*D} = Y_*, \quad \sin \varphi_{bR} = \sin \varphi_L, \quad m_{T'} = m_T = m_{\bar{B}} = m_{\bar{T}}, \quad (13)$$

so that there are five free parameters left: three mixing angles ( $\sin \varphi_L$ ,  $\sin \varphi_{tR}$ ,  $\tan \theta_3$ ) and two masses ( $m_{\bar{T}}$ ,  $M_{G^*}$ ). Alternatively, one can also trade two of the mixing angles,  $\sin \varphi_L$ ,  $\tan \theta_3$ , for the two couplings  $Y_*$ ,  $g_{*3}$ .

## 2.2 Phenomenology of $G^*$

Starting from the rotated lagrangian (27), one can derive the phenomenology of the heavy gluon. The couplings of  $G^*$  to the fermions are reported in eqs.(32)-(35) of Appendix A. In particular,  $G^*$  couples to the light quarks with strength  $(-g_3 \tan \theta_3)$ , and in general with a much stronger coupling to the top, bottom and heavy fermions. Gauge invariance forbids a coupling with two gluons and one  $G^*$  at the level of renormalizable operators. The main rate of production at the LHC hence comes from the Drell-Yan process  $pp \rightarrow q\bar{q} \rightarrow G^*$ . Figure 1 shows the relative cross section for a reference value  $\tan \theta_3 = 0.44$  (corresponding to  $g_{*3} = 3$ ). The analytic expression of the  $G^*$  decay partial widths is given in eqs.(36)-(39) of Appendix A. When kinematically allowed,  $G^*$  can decay to two SM fermions,  $\psi\bar{\psi} = q\bar{q} + t\bar{t} + b\bar{b}$ , where  $q = u, d, c, s$ ; two heavy fermions,  $\chi\bar{\chi}$ , where  $\chi$  denotes any of the heavy fermions; or one heavy plus one SM fermion,  $\psi\bar{\chi} + \chi\bar{\psi} = T\bar{t}_L + B\bar{b}_L + \bar{T}\bar{t}_R + \bar{B}\bar{b}_R + c.c.$ <sup>7</sup> The plot on the left of Fig. 2 shows the relative branching ratios as functions of  $M_{G^*}$  for reference values  $m_{\bar{T}} = 1$  TeV and  $\tan \theta_3 = 0.44$ ,  $\sin \varphi_{tR} = 0.6$ ,  $Y_* = 3$  (hence  $\sin \varphi_L = 0.56$ ). The corresponding total decay width of  $G^*$  is shown in the plot on the right of the same figure, for the same reference values of parameters.

When the decays to one heavy fermion are kinematically forbidden,  $M_{G^*} \lesssim m_{\bar{T}}$ , the heavy gluon can decay only to pairs of SM quarks. The relative importance of the various channels

<sup>5</sup> More specifically, we compute the SM top and bottom masses and all decay widths of the heavy fermions at  $O(r)$ , and we neglect the  $O(r^2)$  EWSB corrections to the masses of the heavy fermions.

<sup>6</sup>In the most extreme case under consideration  $Y_* = 3$ ,  $\bar{m} = 1$  TeV, so that  $r \simeq 3/4$ .

<sup>7</sup>We classify all particles according to their  $SU(2)_L \times U(1)_Y$  quantum numbers, and compute all decay widths at  $O(r)$ . See also footnote 5.

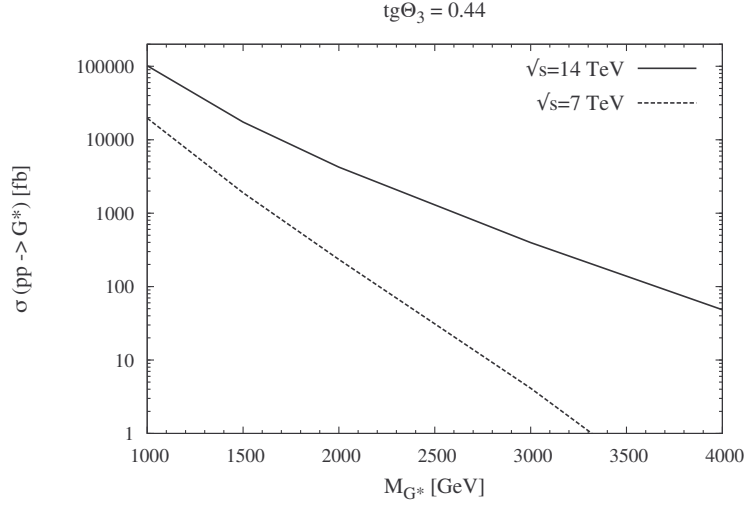


Figure 1: Cross section of the Drell-Yan production of  $G^*$  at the LHC,  $pp \rightarrow q\bar{q} \rightarrow G^*$ , for  $\tan\theta_3 = 0.44$  ( $g_{*3} = 3$ ). For different values of  $\tan\theta_3$  the cross section scales as  $(\tan\theta_3)^2$ .

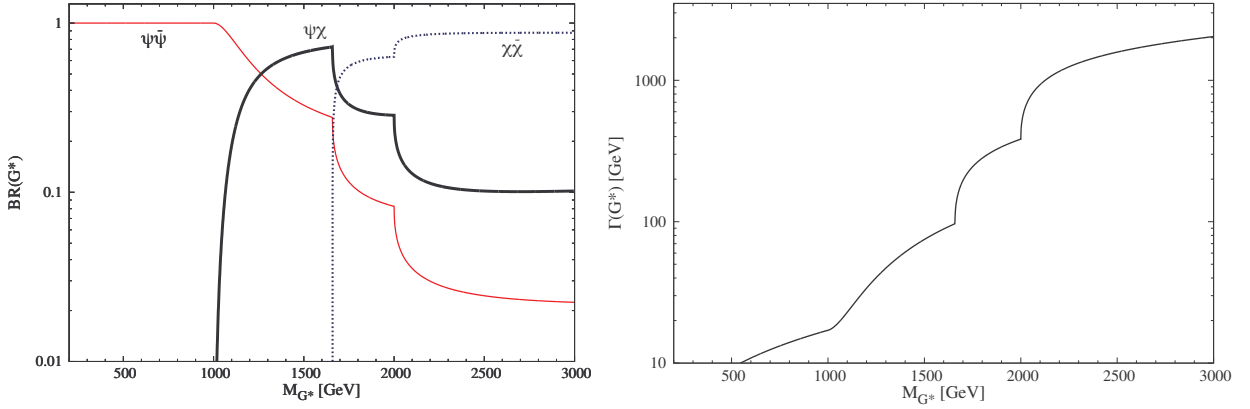


Figure 2: Left plot: branching ratios for the decay of  $G^*$  to two SM fermions,  $\psi\bar{\psi}$ , two heavy fermions,  $\chi\bar{\chi}$ , and one SM plus one heavy fermion,  $\psi\bar{\chi} + \chi\bar{\psi}$ , as a function of  $M_{G^*}$ . Right plot: total decay width of  $G^*$  as a function of  $M_{G^*}$ . Both plots are done setting the other parameters to the following reference values:  $m_{\tilde{T}} = 1$  TeV and  $\tan\theta_3 = 0.44$ ,  $\sin\varphi_{tR} = 0.6$ ,  $Y_* = 3$ .



is controlled by  $\tan \theta_3$  and the top degrees of compositeness  $\sin \varphi_{tR}$ ,  $\sin \varphi_L$ . For small values of  $\tan \theta_3$ , which are naturally implied by the hierarchy of couplings  $g_{el3} \ll g_{*3}$ , or large top degree of compositeness, the dominant channel is  $t\bar{t}$ . For example, for a fully composite  $t_R$ ,  $\sin \varphi_{tR} = 1$ , and  $\tan \theta_3 = 0.2$ ,  $Y_* = 3$  (hence  $\sin \varphi_L = 0.33$ ) one has  $BR(G^* \rightarrow t\bar{t}) = 0.98$ ,  $BR(G^* \rightarrow q\bar{q}) = 0.012$ . In this limit,  $t\bar{t}$  is the best channel to discover the  $G^*$ , despite the huge QCD background [5, 6]. On the other hand, large branching ratios to pairs of light quarks can be obtained even for moderate top degrees of compositeness if  $\tan \theta_3$  is not too small. This is a consequence of the cancellation that can occur between the two terms in eq.(33) due to the relative minus sign. For example, for  $\sin \varphi_{tR} = 0.6$ ,  $\tan \theta_3 = 0.44$ ,  $Y_* = 3$  one has  $BR(G^* \rightarrow t\bar{t}) = 0.18$ ,  $BR(G^* \rightarrow q\bar{q}) = 0.69$ . In this case the strongest discovery reach (or exclusion power) comes from the dijet searches.

For large values of  $M_{G^*}$ , the heavy gluon mostly decays to pairs of heavy fermions, due to the large number of available channels and the large couplings. This is clearly illustrated by the plot on the left of Fig. 2. In this case a first threshold to  $T_{5/3}\bar{T}_{5/3} + T_{2/3}\bar{T}_{2/3}$  opens up at  $M_{G^*} = 2m_{T_{5/3}} = 2m_{\tilde{T}} \cos \varphi_L \simeq 1.66$  TeV, and a second one at  $M_{G^*} = 2m_{\tilde{T}} = 2$  TeV. In this limit the large value of the total decay width that follows for the large multiplicity of decay channels (see the right plot of Fig. 2) makes a discovery of  $G^*$  very challenging.

There is however a third scenario, which is realized for  $m_{\tilde{T}} \lesssim M_{G^*} < 2m_{T_{5/3}}$ . In this case the threshold for decaying to two heavy fermions is kinematically closed, so that the  $G^*$  total width remains small, but decays to one SM fermion plus one heavy fermion are allowed and have a large branching ratio, see Fig. 2. Such heavy-light decays are possible only if the SM fermion and the heavy fermion have the same quantum numbers under  $SU(2)_L \times U(1)_Y$ , that is, the heavy fermion must be one of the partners of the top or bottom:  $\chi = T, B, \tilde{T}, \tilde{B}$ . Due to their large Yukawa coupling, these heavy states mostly decay to one top or bottom plus one longitudinally-polarized vector boson or Higgs boson. The analytic expression of the corresponding decay widths is reported in eqs.(40)-(42) of Appendix A. In the limit  $m_\chi \gg m_t, m_W$ , the branching ratios of the possible decay modes are:

$$\begin{aligned}
BR(T \rightarrow Z_L t_R) &\simeq BR(T \rightarrow h t_R) \simeq 50\%, \\
BR(B \rightarrow W_L t_R) &\simeq 100\%, \\
BR(\tilde{T} \rightarrow W_L b_L) &\simeq 50\%, \quad BR(\tilde{T} \rightarrow Z_L t_L) \simeq BR(\tilde{T} \rightarrow h t_L) \simeq 25\%, \\
BR(\tilde{B} \rightarrow Z_L b_R) &\simeq BR(\tilde{B} \rightarrow h b_R) \simeq 50\%.
\end{aligned} \tag{14}$$

Considering the pattern of decays, we can identify five final channels:

$$Bb, \tilde{T}t \rightarrow Wtb, \quad Tt, \tilde{T}t \rightarrow Zt\bar{t}, \quad Tt, \tilde{T}t \rightarrow ht\bar{t}, \quad \tilde{B}b \rightarrow Zb\bar{b}, \quad \tilde{B}b \rightarrow hb\bar{b}. \tag{15}$$

Their relative importance is shown in Fig. 3 as a function of  $M_{G^*}$ , for the same reference values of parameters chosen for Fig. 2. One can see that each of the heavy-light topologies has a sizable branching ratio in a large range of  $G^*$  masses above  $m_{\tilde{T}}$  and below  $2m_{T_{5/3}}$ , while the  $t\bar{t}$  channel is suppressed compared to its value at  $M_{G^*} < m_{\tilde{T}}$ . Notice that although  $BR(G^* \rightarrow q\bar{q})$  gets suppressed as well, it is still sizable for the benchmark values of parameters chosen in Fig. 3. While large branching fractions for the heavy-light decays are mainly implied by the kinematics and as such are a robust prediction, the value of  $BR(G^* \rightarrow q\bar{q})$  is strongly

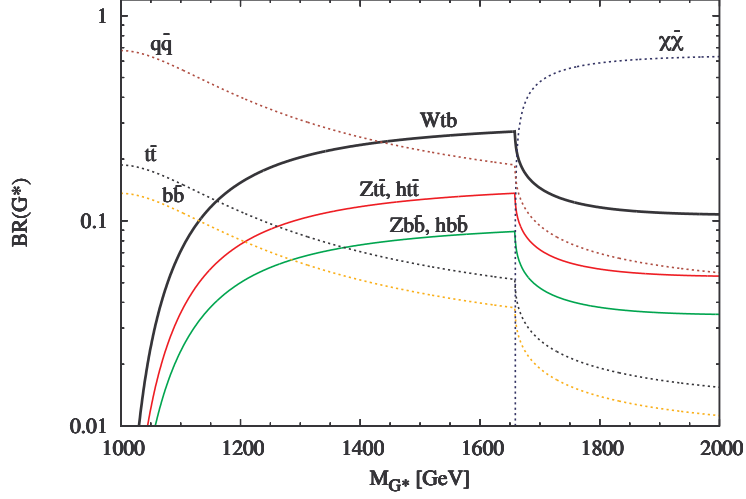


Figure 3: Branching ratio of the various final states that follow from the decay of  $G^*$ , as functions of  $M_{G^*}$ . The other parameters are set to the same reference values used for Fig. 2:  $m_{\tilde{T}} = 1$  TeV and  $\tan \theta_3 = 0.44$ ,  $\sin \varphi_{tR} = 0.6$ ,  $Y_* = 3$ . The decay channel  $ht\bar{t}$  ( $hb\bar{b}$ ) has the same branching ratio of  $Zt\bar{t}$  ( $Zb\bar{b}$ ).

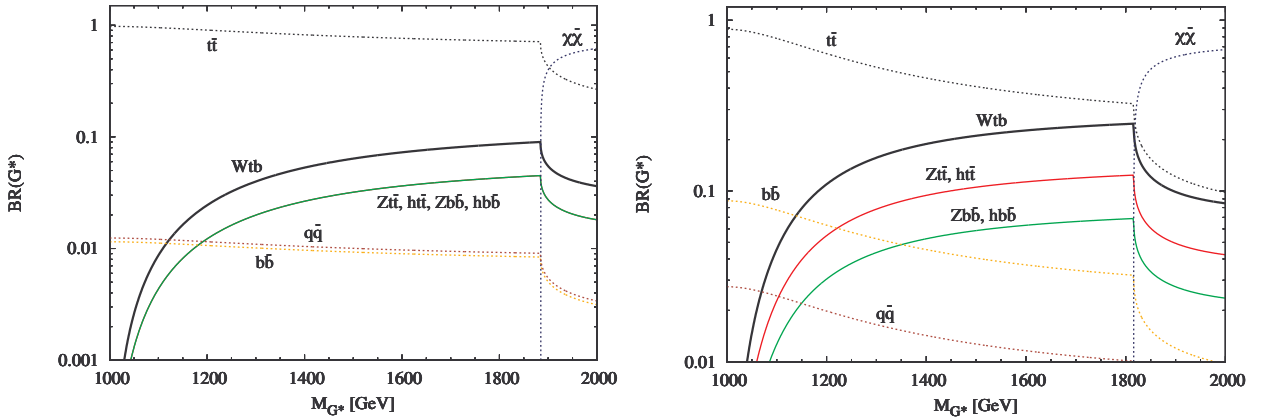


Figure 4: Branching ratios of  $G^*$  to the various final states as functions of  $M_{G^*}$ . Compared to Fig. 3, two different set of parameters have been chosen:  $\sin \varphi_{tR} = 1$ ,  $\tan \theta_3 = 0.2$ ,  $Y_* = 3$ ,  $\sin \varphi_L = 0.33$  (left plot), and  $\sin \varphi_{tR} = 0.8$ ,  $\tan \theta_3 = 0.2$ ,  $Y_* = 3$ ,  $\sin \varphi_L = 0.41$  (right plot). Both plots are done fixing  $m_{\tilde{T}} = 1$  TeV.

dependent on  $\tan\theta_3$  and can thus be easily made small. This is clearly illustrated in Fig. 4, where the branching ratios to the various channels are shown for two different choices of parameters. The left plot refers to the same benchmark point adopted in Ref. [5],  $\sin\varphi_{tR} = 1$ ,  $\tan\theta_3 = 0.2$ ,  $Y_* = 3$  ( $\sin\varphi_L = 0.33$ ); in this case the  $t\bar{t}$  channel largely dominates over the others until the threshold  $M_{G^*} = 2m_{T_{5/3}}$ , as a consequence of the full degree of compositeness of the right-handed top. The right plot refers instead to a similar set of parameters where, however, the degree of compositeness of  $t_R$  is slightly smaller:  $\sin\varphi_{tR} = 0.8$ ,  $\tan\theta_3 = 0.2$ ,  $Y_* = 3$  ( $\sin\varphi_L = 0.41$ ). It is evident how in this case the  $t\bar{t}$  branching ratio is substantially reduced in the range  $m_{\tilde{T}} \lesssim M_{G^*} < 2m_{T_{5/3}}$ , and those of the heavy-light channels, especially  $Wtb$ , are sizable. Notice that in this case the branching ratio of  $q\bar{q}$  is extremely small, as due to the small value of  $\tan\theta_3$ .

Given their numerical importance for  $m_{\tilde{T}} \lesssim M_{G^*} < 2m_{T_{5/3}}$ , the heavy-light decay channels represent a new promising strategy for discovering the  $G^*$ , in a limit in which the latter is still a relatively narrow resonance. The reason is mainly twofold: on the one hand, one can use the peculiar topology of the heavy-light decays, where the invariant mass of a subsystem reconstructs the physical mass of the heavy fermion, to efficiently reduce the QCD background; on the other hand, the  $t\bar{t}$  channel has a much smaller rate for  $m_{\tilde{T}} \lesssim M_{G^*} < 2m_{T_{5/3}}$ , hence it is much less efficient as a discovery channel. Quite remarkably, as it will emerge from our analysis, the heavy-light decays seem extremely competitive channels for discovering the heavy fermions as well. As a final bonus, they also give the opportunity to measure some important features of the fermionic sector, like for example the couplings of the heavy fermions to the SM vector bosons, and thus determine its origin.

Ideally, one could look for the presence of (fermionic) resonances in all the channels of eq.(15). Simple considerations on the size of the SM backgrounds suggest that the most promising final states could be the following (we assume that the Higgs boson is light and mostly decays to  $b\bar{b}$ ):  $Wtb$ ;  $Zt\bar{t}, ht\bar{t} \rightarrow b\bar{b}t\bar{t}$ ;  $Zb\bar{b}, hb\bar{b} \rightarrow 4b$ . A heavy fermion with charge  $+2/3$  will thus appear as a ( $b\bar{b}t$ ) resonance in  $b\bar{b}t\bar{t}$  events, and possibly as a ( $Wb$ ) resonance in  $Wtb$  events if it is a singlet of  $SU(2)_L$  ( $\tilde{T}$ ). The non-observation of this latter signal would in turn point in favor of a classification of the heavy top as part of a doublet of  $SU(2)_L$  ( $T$ ). A heavy fermion with charge  $-1/3$ , on the other hand, will appear as a ( $3b$ ) resonance in  $4b$  events only if it is an electroweak singlet ( $\tilde{B}$ ) and the SM  $b_R$  is not too elementary (this was our assumption when we derived the estimates in eq.(14)). The ( $4b$ ) channel can thus give a way to test the degree of compositeness of  $b_R$ . If  $b_R$  is very much elementary, on the other hand, even a singlet  $\tilde{B}$  will decay mostly to  $Wtb$  events, similarly to a doublet  $B$ . In this case one will observe a ( $Wt$ ) resonance in  $Wtb$  events.

The above discussion shows how a detailed picture on the quantum numbers of the fermionic resonances can be obtained by exploiting all the decay final states. In what follows we will consider the  $Wtb$  channel, which seems to be the most promising one, and we will study it in detail.

### 3 Analysis of the $Wtb$ channel at the LHC

In this section we discuss the prospects of observing the signal in the  $Wtb$  channel at the LHC. We will present a simple parton-level analysis aimed at assessing the LHC discovery reach,

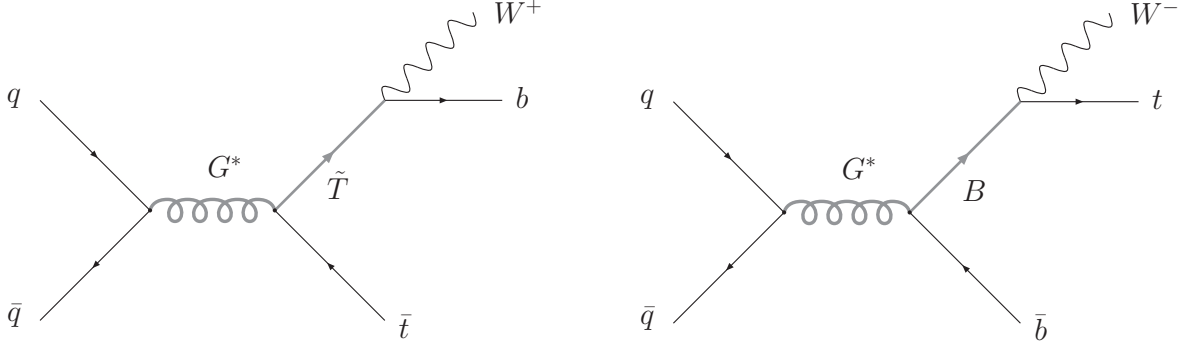


Figure 5: Signal topologies contributing to the  $Wtb$  channel. The conjugate processes proceed through similar diagrams.

and focus on final states with one lepton. Our event selection will be cut-based and driven by simplicity as much as possible. We consider two center-of-mass energies:  $\sqrt{s} = 7$  TeV, the energy of the current phase of data taking, and  $\sqrt{s} = 14$  TeV, the design energy that will be reached in the second phase of operation of the LHC. Our selection strategy and the set of kinematic cuts that we will design are largely independent, however, of the value of the collider energy. This is because they will be optimized to exploit the peculiar kinematics of the signal, and a change in the collider energy mainly implies a rescaling of the production cross sections of signal and background via the parton luminosities, without affecting the kinematic distributions.

There are two signal topologies contributing to the  $Wtb$  channel (see Fig. 5): either the  $G^*$  decays to one SM and one heavy top ( $\tilde{T}$ ), and the latter then decays to  $Wb$ ; or the  $G^*$  decays to one SM and one heavy bottom ( $B$ ) and the latter decays to  $Wt$ . Final states with one lepton thus follow from the decay chains:

$$\begin{aligned}
 q\bar{q} &\rightarrow G^* \rightarrow \tilde{T}\bar{t}_R + c.c. \rightarrow W^+b\bar{t} + c.c. \rightarrow l^\pm\nu b\bar{b}q\bar{q} \\
 q\bar{q} &\rightarrow G^* \rightarrow B\bar{b}_L + c.c. \rightarrow W^-t\bar{b} + c.c. \rightarrow l^\pm\nu b\bar{b}q\bar{q}.
 \end{aligned}
 \tag{16}$$

The physical, observed process is  $pp \rightarrow l^\pm + jets + \cancel{E}_T$ , with up to four jets from the hard scattering, two of which are  $b$ -jets. The same final state can however follow from another signal topology, where  $G^*$  decays to  $t\bar{t}$ :

$$q\bar{q} \rightarrow G^* \rightarrow t\bar{t} \rightarrow W^+bW^-\bar{b} \rightarrow l^\pm\nu b\bar{b}q\bar{q}.
 \tag{17}$$

This is the decay chain on which previous studies aimed at the discovery of the  $G^*$  focussed.

As a reference model for the signal we will consider the two-site model TS5 described in the previous section. As explained there, since the decay rates of  $T \rightarrow Wb_R$  and  $\tilde{B} \rightarrow Wt_L$  are strongly suppressed in the TS5 (see eq.(14)), the decay chains  $q\bar{q} \rightarrow G^* \rightarrow T\bar{t} + \tilde{B}\bar{b} + c.c. \rightarrow Wtb$  give a negligible contribution and will not be included in the following. We perform our analysis adopting the following benchmark values of parameters ( $m_h$  is the Higgs mass)

$$\begin{aligned}
 Y_* = g_{*3} = 3, \quad \sin\varphi_{t_R} = 0.6 \quad (\text{which implies: } \tan\theta_3 = 0.44, \sin\varphi_L = 0.55) \\
 \frac{M_{G^*}}{m_{\tilde{T}}} = 1.5, \quad M_{G^*} = 1.5, 2.0, 3.0, 4.0 \text{ TeV}, \quad m_h = 120 \text{ GeV},
 \end{aligned}
 \tag{18}$$

$M_{G^*} [\text{TeV}]$	$\sigma(pp \rightarrow G^*)$	
	$\sqrt{s} = 7 \text{ TeV}$	$\sqrt{s} = 14 \text{ TeV}$
1.5	1.90 pb	17.4 pb
2.0	234 fb	4.23 pb
3.0	4.12 fb	397 fb
4.0	0.05 fb	48.3 fb

Table 1: Values of the  $G^*$  production cross section at the LHC for the benchmark choice of parameters of eq.(18).

and we make a simple extrapolation to different values at the end. In particular, we fix the ratio of the  $G^*$  mass over the heavy fermion mass to  $M_{G^*}/m_{\tilde{T}} = 1.5$ , within the interval  $m_{\tilde{T}} < M_{G^*} < 2m_{T_{5/3}}$  where the processes of eq.(16) are kinematically allowed and fast. For the reader's convenience, we report in Table 1 the values of the  $G^*$  production cross section at the benchmark points of eq.(18) (see also Fig. 1). The particles' total decay widths are

$$\frac{\Gamma(G^*)}{M_{G^*}} = 0.052, \quad \frac{\Gamma(\tilde{T})}{m_{\tilde{T}}} = 0.035, \quad \frac{\Gamma(B)}{m_B} = 0.022, \quad (19)$$

and the branching ratios of the  $Wtb$  and  $t\bar{t}$  channels are <sup>8</sup>

$$\begin{aligned} BR(G^* \rightarrow Bb \rightarrow Wtb) &= 0.17 \\ BR(G^* \rightarrow \tilde{T}t \rightarrow Wtb) &= 0.08 \\ BR(G^* \rightarrow t\bar{t}) &= 0.06. \end{aligned} \quad (20)$$

Hence, approximately two thirds (one third) of the  $Wtb$  events that follow from a heavy-light decay of  $G^*$  is from  $G^* \rightarrow Bb$  ( $G^* \rightarrow \tilde{T}t$ ).

The benchmark values of eq.(18) have been chosen so as to have a large rate in the heavy-light channels. This particular choice however also implies a large branching ratio to a pair of light SM quarks,  $BR(G^* \rightarrow q\bar{q}) = 0.22$  (see Fig. 3), so that the dijet searches will also have a large discovery (or exclusion) power. <sup>9</sup> As previously explained in section 2.2, this is not generic to the model, and it does not occur for other choices of the parameters, like that of the left plot of Fig. 4, which implies large branching ratios for the heavy-light channels and a very small one for  $q\bar{q}$ .

<sup>8</sup>Here and in the following we use the short notation  $G^* \rightarrow Bb + \tilde{T}t$  to denote  $G^* \rightarrow B\bar{b} + \tilde{T}\bar{t} + c.c.$

<sup>9</sup>In fact, the benchmark point (18) might be already excluded, although just marginally, by the bounds from the dijet searches reported by the CMS and ATLAS collaborations [12,13] during the completion of this work. This is what suggests a naive rescaling of the bounds on axigluons and colorons shown in Refs. [12,13]. A more accurate derivation is however required to precisely determine the impact of the dijet searches on the parameter space of our model. We leave this to a future study.

### 3.1 Montecarlo simulation of signal and background

We simulate the signal by using MadGraph v4 [57], while for the background (see discussion below) we make use of both MadGraph and ALPGEN [58].<sup>10</sup> In our parton-level analysis jets are identified with the quarks and gluons from the hard scattering. If two quarks or gluons are closer than the separation  $\Delta R = 0.4$ , they are merged into a single jet whose four-momentum is the vectorial sum of the original momenta. We require that the jets and the leptons satisfy the following set of acceptance and isolation cuts:

$$\begin{aligned} p_{Tj} &\geq 30 \text{ GeV} & |\eta_j| &\leq 5 & \Delta R_{jj} &\geq 0.4 \\ p_{Tl} &\geq 20 \text{ GeV} & |\eta_l| &\leq 2.5 & \Delta R_{jl} &\geq 0.4. \end{aligned} \tag{21}$$

Here  $p_{Tj}$  ( $p_{Tl}$ ) and  $\eta_j$  ( $\eta_l$ ) are respectively the jet (lepton) transverse momentum and pseudorapidity, and  $\Delta R_{jj}$ ,  $\Delta R_{jl}$  denote the jet-jet and jet-lepton separations. Jets that fail the  $p_T$  cut of eq.(21), as well as leptons that fail the isolation and  $p_T$  cut, are discarded and not considered in the reconstruction of the event.  $b$ -jets are assumed to be correctly tagged with an efficiency  $\varepsilon_b = 0.6$  if their pseudorapidity satisfies  $|\eta_b| \leq 2.5$ . We set the corresponding rejection rate on light jets to  $\zeta_b = 100$ .<sup>11</sup>

Detector effects are roughly accounted for by performing a simple Gaussian smearing on the jet energy and momentum absolute value with  $\Delta E/E = 100\%/\sqrt{E/\text{GeV}}$ , and on the jet momentum direction using an angle resolution  $\Delta\phi = 0.05$  radians and  $\Delta\eta = 0.04$ . Moreover, the missing energy  $\cancel{E}_T$  of each event has been computed by including a Gaussian resolution  $\sigma(\cancel{E}_T) = a \cdot \sqrt{\sum_i E_T^i/\text{GeV}}$ , where  $\sum_i E_T^i$  is the scalar sum of the transverse energies of all the reconstructed objects (electrons, muons and jets). We choose  $a = 0.49$ .<sup>12</sup>

Table 2 shows the fraction of  $G^* \rightarrow Bb + \tilde{T}t$  events where the jet content is reconstructed to be respectively  $2j + 2b$ ,  $1j + 2b$ ,  $1j + 1b$  (where  $j$  denotes a light jet) for different values of the  $G^*$  mass and  $\sqrt{s} = 14$  TeV. Very similar numbers hold for  $\sqrt{s} = 7$  TeV. In the third column, the numbers in parenthesis show the relative fraction of  $1j + 2b$  events in which the light jet originates from the merging of the  $q\bar{q}$  pair from the hadronic  $W$ . As naively expected due to the increasing boost of all the decay products, the number of events with four jets decreases for larger  $G^*$  masses, while the fraction of events in which the hadronic  $W$  is reconstructed as a single jet increases. For this reason in our analysis *we will select events with at least three jets and exactly one lepton and two b-tags*:

$$pp \rightarrow l^\pm + n \text{ jets} + \cancel{E}_T, \quad n \geq 3, \quad 2 \text{ b-tags} \tag{22}$$

where all objects must satisfy the acceptance and isolation cuts of eq.(21). Most likely, the use of boosted jet techniques<sup>13</sup> can lead to a better sensitivity on events with three jets,

<sup>10</sup>The choice of MadGraph to simulate the signal is dictated by the possibility of easily implementing our model. For the background, we have used ALPGEN to simulate processes with a large number of particles from the hard scattering. The factorization and renormalization scales have been set to be equal and chosen as follows:  $Q = M_{G^*}$  for the signal;  $Q = \sqrt{m_W^2 + \sum_j p_{Tj}^2}$  for  $WWbb$ ;  $Q = \sqrt{m_W^2 + p_{TW}^2}$  for  $Wbbj$ ,  $Wbbjj$ ,  $Wbb3j$ ,  $W3j$  and  $W4j$ .

<sup>11</sup>The rejection rate corresponds to the inverse of the probability of mistagging a light jet as a  $b$ -jet.

<sup>12</sup>The numerical values of the above parameters, as well as the  $b$ -tagging efficiency and rejection rate, have been chosen according to the performance of the ATLAS detector [59].

<sup>13</sup>See for example the report prepared for the BOOST2010 workshop [60] for a review and a complete list of references.

$M_{G^*}$	$2j + 2b$	$1j + 2b$	$1j + 1b$
1.5 TeV	0.42	0.31 (58%)	0.07
2.0 TeV	0.29	0.42 (79%)	0.10
3.0 TeV	0.13	0.52 (89%)	0.17
4.0 TeV	0.07	0.53 (93%)	0.25

Table 2: Fraction of  $G^* \rightarrow Bb + \tilde{T}t$  events where the jet content is reconstructed to be respectively  $2j + 2b$ ,  $1j + 2b$ ,  $1j + 1b$  (where  $j$  denotes a light jet) as a function of the  $G^*$  mass for  $\sqrt{s} = 14$  TeV. In the third column, the numbers in parenthesis show the relative fraction of  $1j + 2b$  events in which the light jet originates from the merging of the  $q\bar{q}$  pair from the hadronic  $W$ .

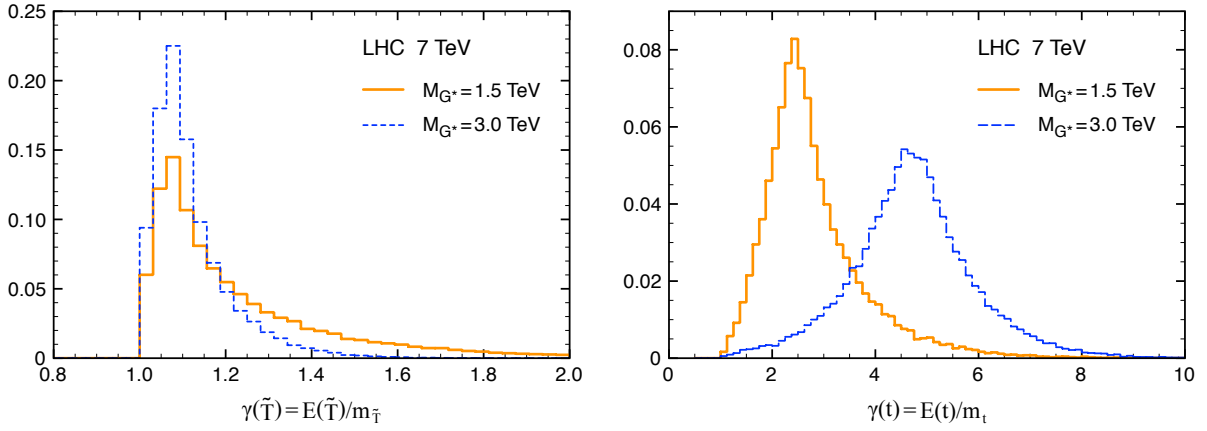


Figure 6: Distribution of the boost factor  $\gamma = E/m$  of  $\tilde{T}$  (left plot) and of the top quark (right plot) in signal events  $G^* \rightarrow \tilde{T}t$  with  $M_{G^*} = 1.5$  TeV (continuous orange line) and  $M_{G^*} = 3.0$  TeV (dashed blue line) for  $\sqrt{s} = 7$  TeV. Notice that having set  $M_{G^*}/m_{\tilde{T}} = 1.5$  implies that  $\tilde{T}$  is less boosted for  $M_{G^*} = 3.0$  TeV than for  $M_{G^*} = 1.5$  TeV. All the curves have been normalized to unit area.

and allow the study of the extreme case, most probable at high  $G^*$  masses, in which the hadronically decayed top is reconstructed as a single fat jet. Notice, on the other hand, that while the SM (top or bottom) quark originating from the  $G^*$  decay is always highly boosted, for  $m_{G^*}/m_{\tilde{T}} = 1.5$  the heavy quark is not. This is clearly shown by Fig. 6 in the case of  $G^* \rightarrow \tilde{T}t$  events. As a consequence, an event selection strategy which relies on a large boost of *all* the decay products, adopted for example by some of the LHC searches for heavy resonances decaying to  $t\bar{t}$ , might have a poor efficiency on our signal.

The largest SM background after the event selection of eq.(22) is the irreducible background  $WWbb$ , which includes the resonant sub-processes  $Wtb \rightarrow WWbb$  (single top) and  $t\bar{t} \rightarrow WWbb$ . The latter, in particular, gives the largest contribution. We have simulated the  $WWbb$  events by using MadGraph. Another background which will turn out to be important after imposing our full set of kinematic cuts is  $Wbb + jets$ . We have simulated  $Wbbj$ ,  $Wbbjj$  and  $Wbb3j$  (this latter process only for  $\sqrt{s} = 14$  TeV) using ALPGEN. Including all these samples with increasing multiplicity of light jets in the final state is redundant, and in

principle leads to a double counting of kinematic configurations. A correct procedure would be resumming soft and collinear emissions by means of a parton shower, and adopting some matching technique to avoid double counting. For simplicity, in our analysis we retain all the  $Wbb + n \text{ jets}$  samples; in this way we expect to obtain a conservative estimate of the background. Notice also that some of the cuts we will impose tend to suppress the events with larger number of jets and thus to reduce the amount of double counting. Finally, the last background that we have considered is  $W + \text{jets}$ , where two light jets are mistagged as  $b$ -jets. We have generated the processes  $W3j$  and  $W4j$  with ALPGEN. As for the  $Wbb + \text{jets}$  background, we conservatively include both these sample. In this case, however, the issue of double counting can be safely ignored since the  $W + \text{jets}$  background will turn out to be much smaller than the others at the end of our analysis.

We did not include other reducible backgrounds which are expected to be subdominant, in particular:  $b\bar{b} + \text{jets}$  where one light jets is misreconstructed as a lepton (it should be possible to reduce it down to a negligible level by requiring enough missing energy in the event); single-top processes  $t + \text{jets}$ ,  $t\bar{b} + \text{jets}$ ,  $Wt + \text{jets}$  (after the request of two  $b$ -tags all these are expected to be much smaller than the single-top background  $Wtb$ ,<sup>14</sup> which is included in our analysis).

While our analysis is carried out at the parton level, we expect it to be robust against the inclusion of detector and showering effects. Our simple Gaussian smearing of the jets' energy and momentum should correctly reproduce the main impact of detector effects on our event selection and reconstruction. The request of two  $b$ -tags and the kinematic cuts that we will impose (like for example on the invariant mass of the hadronic  $W$ , see next section) should reduce the effect of extra radiation in the signal. A detailed study of initial and final state radiation, underlying event and multiple parton collisions is beyond the scope of the present paper and is left for future analyses.

## 3.2 Event selection

The second column of Tables 3 and 4 reports the value of the cross section for the signal and the main SM backgrounds after the selection (22) based on the acceptance and isolation cuts of eq.(21), respectively for  $\sqrt{s} = 7 \text{ TeV}$  and  $14 \text{ TeV}$ . One can see that at this stage the background dominates by far over the signal. We can however exploit the peculiar kinematics of the signal to perform a first set of cuts and reduce the background to a much smaller level without touching the signal.

One basic feature of the signal is that the lepton and the jets in the event tend to be very energetic, as they are the final products of the decay chain of a new heavy particle (either the  $G^*$  or the heavy fermion). This is evident for example from the plots of Fig. 7, which show the  $p_T$  of the leading jet ( $j_1$ ) and of the next-to-leading jet ( $j_2$ ) for the signal at  $M_{G^*} = 1.5 \text{ TeV}$  and for the total background. We will impose a cut on  $p_T(j_{1,2})$  in the following, see eqs.(23),(24).

In order to fully exploit the specific topology of the signal, however, it is convenient to reconstruct the intermediate  $Wtb$  state that follows from the decay of the  $G^*$  and of the heavy fermion, see Fig. 5. To do this, we first reconstruct the longitudinal momentum of

---

<sup>14</sup>See for example Table 32 at page 32 of Ref. [58].



LHC $\sqrt{s} = 7$ TeV		acceptance	$\nu + \text{top rec.}$	zero-cost
$M_{G^*} = 1.5$ TeV	$G^* \rightarrow \tilde{T}t + Bb$	29.8	23.8	22.2
	$G^* \rightarrow t\bar{t}$	5.85	4.72	3.21
$M_{G^*} = 2.0$ TeV	$G^* \rightarrow \tilde{T}t + Bb$	3.29	2.59	2.51
	$G^* \rightarrow t\bar{t}$	0.71	0.56	0.34
$M_{G^*} = 3.0$ TeV	$G^* \rightarrow \tilde{T}t + Bb$	0.04	0.03	0.03
	$G^* \rightarrow t\bar{t}$	0.06	0.05	0.02
	$WWbb$	4838	3932	167
	$Wbbj$	210	156	7.78
	$Wbbjj$	102	67.5	2.17
	$W3j$	18.8	14.5	0.83
	$W4j$	8.89	6.36	0.31
	Total background	5177	4177	179

Table 3: Cross sections, in fb, at  $\sqrt{s} = 7$  TeV for the signal and the main backgrounds after the selection (22) based on the acceptance cuts of eq.(21) (second column); after the neutrino and top quark reconstruction (third column); after imposing the ‘zero-cost’ cuts of eq.(23) (fourth column). For each channel, the proper branching ratio to a one-lepton final state has been included.

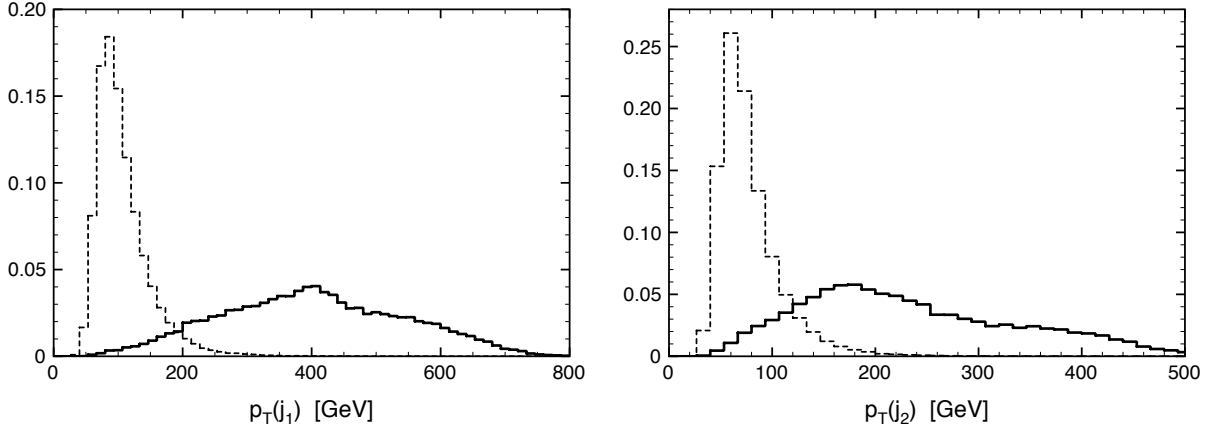


Figure 7: Differential distribution of the  $p_T$  of the leading jet (left plot) and next-to-leading jet (right plot) after the acceptance cuts of eq.(21) for  $\sqrt{s} = 7$  TeV. The continuous line and the dashed line respectively show the signal at  $m_{G^*} = 1.5$  TeV and the total background. All the curves have been normalized to unit area.

LHC $\sqrt{s} = 14$ TeV		acceptance	$\nu + \text{top rec.}$	zero-cost
$M_{G^*} = 1.5$ TeV	$G^* \rightarrow \tilde{T}t + Bb$	262	209	192
	$G^* \rightarrow t\bar{t}$	42.6	34.8	23.7
$M_{G^*} = 2.0$ TeV	$G^* \rightarrow \tilde{T}t + Bb$	56.9	45.0	42.7
	$G^* \rightarrow t\bar{t}$	7.00	5.76	3.93
$M_{G^*} = 3.0$ TeV	$G^* \rightarrow \tilde{T}t + Bb$	3.80	2.95	2.91
	$G^* \rightarrow t\bar{t}$	0.46	0.38	0.22
$M_{G^*} = 4.0$ TeV	$G^* \rightarrow \tilde{T}t + Bb$	0.32	0.24	0.24
	$G^* \rightarrow t\bar{t}$	0.08	0.07	0.03
	$WWbb$	27671	22383	724
	$Wbbj$	794	573	25.9
	$Wbbjj$	574	354	9.30
	$Wbb3j$	215	119	0.63
	$W3j$	67.6	51.3	2.90
	$W4j$	41.2	28.2	1.15
	Total background	29363	23509	764

Table 4: Cross sections, in fb, at  $\sqrt{s} = 14$  TeV for the signal and the main backgrounds after the selection (22) based on the acceptance cuts of eq.(21) (second column); after the neutrino and top quark reconstruction (third column); after imposing the ‘zero-cost’ cuts of eq.(24) (fourth column). For each channel, the proper branching ratio to a one-lepton final state has been included.

the neutrino, up to a twofold ambiguity, by enforcing the on-shell condition  $m(l\nu) = m_W$ . Events where the second-order equation has no (real) solution are removed.<sup>15</sup> We thus have two pairs  $(l\nu)$ , one for each neutrino solution, which represent our two candidates for the first  $W$  in the signal:  $W_{l_{1,2}} = (l\nu_{1,2})$ . Next, we use the fact that in the signal there is a second  $W$  that decays hadronically, and label all the jets other than the two  $b$ -jets to form our hadronic  $W$  candidate,  $W_h$ . Notice that in events with exactly three hard jets,  $W_h$  will consist of a single jet. Starting from the three  $W$  candidates and the two  $b$ -jets in the event, there are six  $(Wb)$  pairs that one can form. We select the pair whose invariant mass is closest to the top quark mass, and label it as our top quark candidate:  $(W_t b_t)$ . The remaining  $b$  and  $W$  candidates will be labeled as  $b_\cancel{y}$  and  $W_{\cancel{y}}$ , since in the signal they do not come from the decay of a top quark. In the case in which the  $W$  selected as belonging to the top quark is one of the two leptonic candidates,  $W_t = W_{l_i}$ , the other leptonic candidate is discarded. In other words, the top reconstruction in this case gives us a criterion to select one of the two neutrino solutions. If instead the  $W$  selected as belonging to the top quark is the hadronic one,  $W_t = W_h$ , then both the remaining  $W$  candidates are kept. As a first loose cut on the invariant mass of the reconstructed top we require  $80 \text{ GeV} < m(W_t b_t) < 250 \text{ GeV}$ . The efficiency of this cut on the signal and on the backgrounds with at least one top quark is  $\sim 100\%$ . The value of the cross sections after both the neutrino and top reconstruction are reported in the third column of Tables 3 and 4.

The identification of the  $Wtb$  intermediate state allows us to fully take advantage of the peculiarity of the signal, where each of these three SM particles is extremely energetic. This is illustrated by Fig. 8, which shows the distributions of the transverse momenta of the reconstructed top,  $p_T(W_t b_t)$ , and of the  $W$  candidate and  $b$ -jet not belonging to it,  $p_T(W_\cancel{y})$ ,  $p_T(b_\cancel{y})$ , at  $\sqrt{s} = 7 \text{ TeV}$ . Also shown is the distribution of the invariant mass of the hadronic  $W$  candidate,  $m(W_h)$ . Similar plots are obtained for  $\sqrt{s} = 14 \text{ TeV}$ . As a first set of cuts, we thus use the kinematic observables of Figs. 7, 8. At  $\sqrt{s} = 7 \text{ TeV}$  we require:

$$\begin{aligned}
p_T(j_1) &\geq 155 \text{ GeV} & p_T(j_2) &\geq 75 \text{ GeV} & m(W_h) &\leq 200 \text{ GeV} \\
p_T(W_t b_t) &\geq 105 \text{ GeV} & p_T(W_\cancel{y}) &\geq 90 \text{ GeV} & p_T(b_\cancel{y}) &\geq 65 \text{ GeV},
\end{aligned}
\tag{23}$$

while at  $\sqrt{s} = 14 \text{ TeV}$  we impose slightly stronger cuts as follows:

$$\begin{aligned}
p_T(j_1) &\geq 175 \text{ GeV} & p_T(j_2) &\geq 85 \text{ GeV} & m(W_h) &\leq 200 \text{ GeV} \\
p_T(W_t b_t) &\geq 110 \text{ GeV} & p_T(W_\cancel{y}) &\geq 110 \text{ GeV} & p_T(b_\cancel{y}) &\geq 70 \text{ GeV}.
\end{aligned}
\tag{24}$$

In each case, the numerical values of the cuts have been chosen so that each cut individually reduces the signal  $G^* \rightarrow \tilde{T}t + Bb$  at  $M_{G^*} = 1.5 \text{ TeV}$  by no more than  $\sim 2\%$ , so that they are basically at ‘zero cost’ for the signal. Notice that when two  $W_\cancel{y}$  candidates exist, by construction they have the same transverse momentum, so that the cut on  $p_T(W_\cancel{y})$  of eqs.(23),(24) applies to either of them. As clearly illustrated by Fig. 8, the cut on  $m(W_h)$  is useful to reduce the backgrounds that do not have a second  $W$ , in particular  $Wbb + jets$  and  $W + jets$ .

---

<sup>15</sup>Although this algorithm is very rough and does not account for the amount of off-shellness of the  $W$  boson, it has a sufficiently large efficiency on our signal:  $\varepsilon_\nu \sim 0.8$ . We do not attempt here to adopt more refined strategies, which are however well known and can be easily implemented in a full analysis.

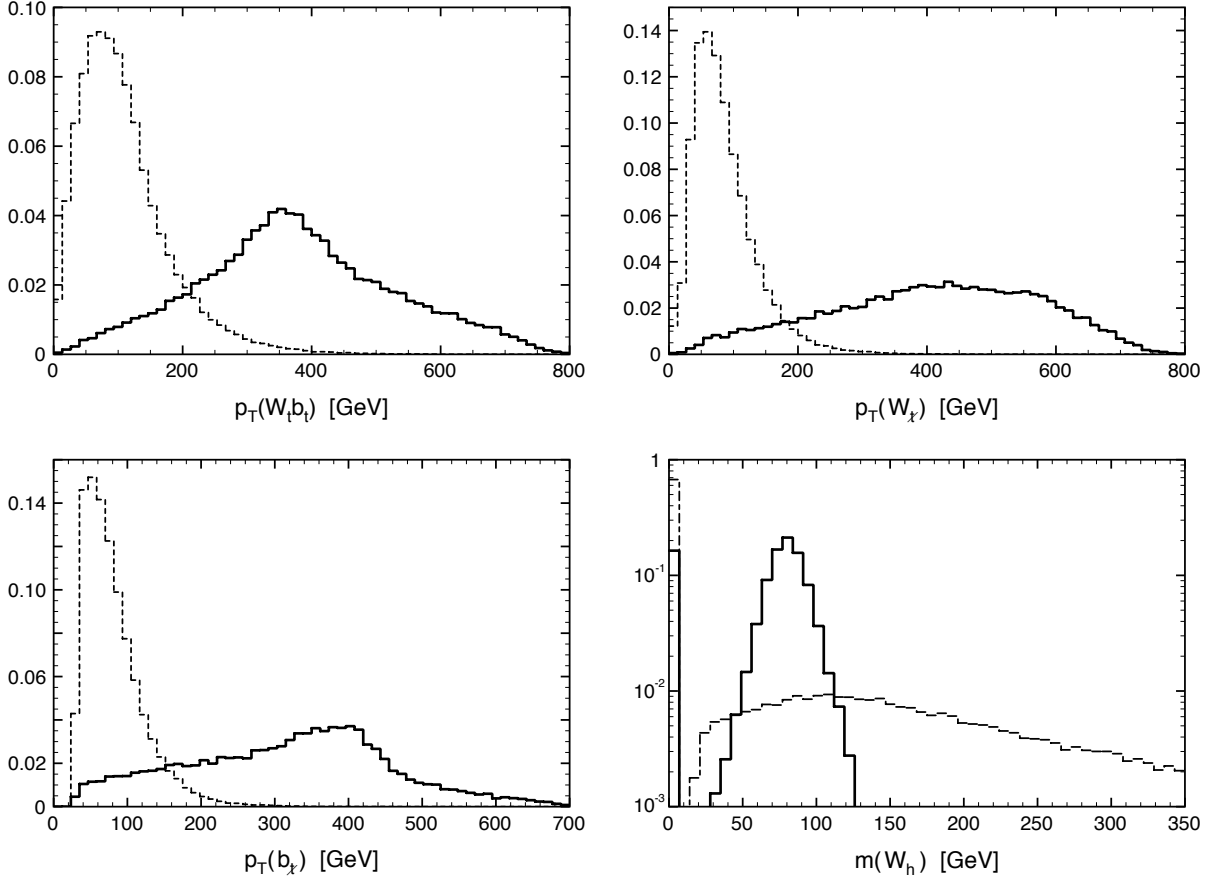


Figure 8: Differential distributions after the neutrino and top reconstruction for  $\sqrt{s} = 7$  TeV. Upper left plot:  $p_T$  of the top candidate,  $p_T(W_t b_t)$ ; Upper right plot:  $p_T$  of the  $W$  candidate labeled as not belonging to the top quark,  $p_T(W_j)$  (if two such candidates exist they have the same transverse momentum by construction, see text); Lower left plot:  $p_T$  of the  $b$ -jet labeled as not belonging to the top quark,  $p_T(b_j)$ ; Lower right plot: invariant mass of the hadronic  $W$  candidate,  $m(W_h)$ . In this latter plot, the first bin is populated by events with exactly three jets, for which  $m(W_h) = 0$  in our partonic analysis. The continuous line shows the signal at  $m_{G^*} = 1.5$  TeV; in the upper plots and the lower left plot, the dashed line shows the total background; in the lower right plot, the dashed line shows the (sum of the) backgrounds without a second  $W$ , namely  $Wbb + jets$  and  $W + jets$ . All the curves have been normalized to unit area.

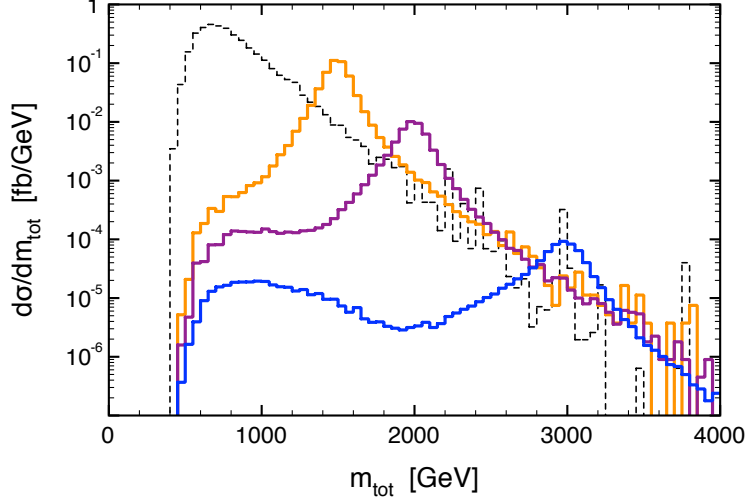


Figure 9: Differential cross section as a function of the total invariant mass of the  $Wtb$  system,  $m_{tot} \equiv m(W_t b_t W_{\not{t}} b_{\not{t}})$ , after the cuts at ‘zero cost’ of eq.(23) at  $\sqrt{s} = 7$  TeV. The dashed curve denotes the total background; the orange, purple, and blue continuous curves denote the signal respectively at  $M_{G^*} = 1.5, 2.0, 3.0$  TeV. The long tail of the signal curves at low  $m_{tot}$  is due to events with an off-shell  $G^*$ . When two  $W_l$  candidates exist in an event, the corresponding two solutions for  $m_{tot}$  have been both included, each with weight  $1/2$ .

The cross sections of the signal and the backgrounds after the cuts at ‘zero cost’ of eq.(23) and (24) are reported in the fourth column of respectively Table 3 and 4. At this stage, although the background has been strongly reduced, it is still dominant over the signal. In particular, the largest background comes from the resonant contribution  $t\bar{t} \rightarrow WWbb$ . An obvious strategy to suppress it, adopted in previous analyses aimed at uncovering the signal  $G^* \rightarrow t\bar{t}$ , is that of cutting on the total invariant mass of the event. This is illustrated by Fig. 9, which shows the differential cross sections of the signal and of the total background for  $\sqrt{s} = 7$  TeV as functions of the invariant mass of the  $Wtb$  system after the cuts of eq.(23). Obtaining a better significance of the  $G^* \rightarrow t\bar{t}$  signal over the background, especially at large  $G^*$  masses and widths, requires additional and more sophisticated tools, like for the example the use of a left-right polarization asymmetry [5, 6]. The peculiar topology of the process  $G^* \rightarrow \tilde{T}t + Bb$ , on the other hand, suggests a further simple strategy, namely requiring that the invariant mass of the  $(W_{\not{t}} b_{\not{t}})$  system be much bigger than the top mass  $m_t$ . In the case of  $G^* \rightarrow \tilde{T}t$ , indeed,  $m(W_{\not{t}} b_{\not{t}})$  peaks at  $m_{\tilde{T}}$ , and even in  $G^* \rightarrow Bb$  events it tends to be much larger than  $m_t$ . This is shown by the contour plot of Fig. 10, which reports the isocurves of the (doubly differential) cross section in the plane  $(m_{tot}, m_{Wb})$ , where  $m_{Wb} \equiv m(W_{\not{t}} b_{\not{t}})$  and  $m_{tot} \equiv m(W_{\not{t}} b_{\not{t}} W_t b_t)$ . By simple inspection, one can see that the SM  $t\bar{t}$  background can be strongly reduced by cutting at the same time on  $m_{tot}$  and on  $m_{Wb}$ . We find that an additional cut on  $m_{Wt} \equiv m(W_{\not{t}} W_t b_t)$  is useful at large  $M_{G^*}$  to further reduce the background and increase the signal significance, see Fig. 11. Although cutting on  $m_{Wb}$  removes almost entirely the  $t\bar{t}$  component of the signal, this can still be detected by adopting the strategies proposed in previous analyses. In the following, instead, we will focus on the  $G^* \rightarrow \tilde{T}t + Bb$  signal.

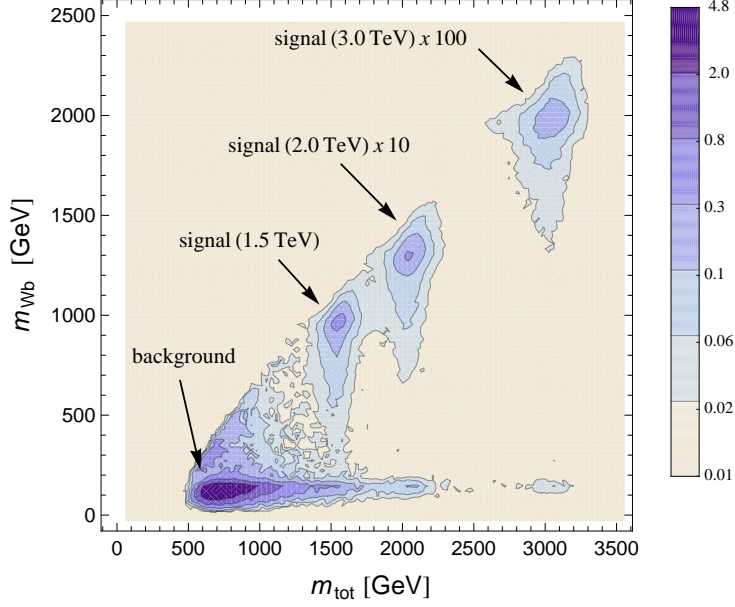


Figure 10: Contour plot of the signal and total background cross sections after the cuts at ‘zero cost’ of eq.(23) in the plane  $(m_{tot}, m_{Wb})$ , where  $m_{Wb} \equiv m(W_{\not{p}}b_{\not{p}})$  and  $m_{tot} \equiv m(W_{\not{p}}b_{\not{p}}W_t b_t)$ . The center-of-mass energy is  $\sqrt{s} = 7$  TeV. Different colors correspond to areas of different values of the doubly differential cross section  $d^2\sigma/dm_{Wb}dm_{tot}$ , as reported in the vertical color key on the right in units  $\text{ab}/\text{GeV}^2$ . The signals at  $M_{G^*} = 2.0$  TeV and 3.0 TeV have been rescaled respectively by a factor 10 and 100.

For each value of  $M_{G^*}$  we find a set of optimized cuts that minimizes the integrated luminosity needed for a  $5\sigma$  discovery.<sup>16</sup> These are:

$$\begin{aligned}
 \underline{M_{G^*} = 1.5 \text{ TeV}} : \quad & m_{tot} \geq 1300 \text{ GeV} \quad m_{Wb} \geq 400 \text{ GeV} \\
 \underline{M_{G^*} = 2.0 \text{ TeV}} : \quad & m_{tot} \geq 1700 \text{ GeV} \quad m_{Wb} \geq 600 \text{ GeV} \\
 \underline{M_{G^*} = 3.0 \text{ TeV}} : \quad & m_{tot} \geq 2500 \text{ GeV} \quad m_{Wb} \geq 600 \text{ GeV} \quad m_{Wt} \geq 700 \text{ GeV} \\
 \underline{M_{G^*} = 4.0 \text{ TeV}} : \quad & m_{tot} \geq 3200 \text{ GeV} \quad m_{Wb} \geq 700 \text{ GeV} \quad m_{Wt} \geq 900 \text{ GeV} .
 \end{aligned} \tag{25}$$

In each case, the efficiency of the cut on  $m_{Wb}$  *after* imposing that on  $m_{tot}$  is of the order of a few percent for the  $WWbb$  background, and  $\sim 90\%$  for the  $G^* \rightarrow \tilde{T}t + Bb$  signal. The values of the cross sections after these optimized cuts are reported in Tables 5 and 6 (in the columns labeled as ‘OPT’) respectively for  $\sqrt{s} = 7$  TeV and 14 TeV. The values of the corresponding discovery luminosity are reported in Table 7.

<sup>16</sup> We define the discovery luminosity to be the integrated luminosity for which a goodness-of-fit test of the SM-only hypothesis with Poisson distribution gives a p-value =  $2.85 \times 10^{-7}$ , which corresponds to a  $5\sigma$  significance in the limit of a gaussian distribution. If however this value is less than the luminosity for which the total (signal plus background) number of expected events is equal to 10, this latter value is conservatively defined as the discovery luminosity.

LHC 7 TeV	$M_{G^*} = 1.5 \text{ TeV}$		$M_{G^*} = 2.0 \text{ TeV}$		$M_{G^*} = 3.0 \text{ TeV}$
	OPT	OPT(II)	OPT	OPT(II)	OPT
$G^* \rightarrow \tilde{T}t + Bb$	20.0(1)	14.9(1)	2.28(1)	1.85(1)	0.0301(2)
$WWbb$	0.17(6)	0.06(4)	0.06(4)	0.02(3)	< 0.03
$Wbbj$	0.32(2)	0.13(1)	0.044(7)	0.022(5)	0.003(2)
$Wbbjj$	0.11(2)	0.06(1)	0.023(8)	0.008(5)	0.003(4)
$W3j$	0.082(3)	0.036(2)	0.018(2)	0.008(1)	0.0009(3)
$W4j$	0.039(3)	0.015(2)	0.011(1)	0.005(1)	0.0004(4)
Total background	0.72(7)	0.29(4)	0.15(4)	0.06(3)	$0.007^{+0.03}_{-0.004}$

Table 5: Cross sections, in fb, at  $\sqrt{s} = 7 \text{ TeV}$  for the signal and the main backgrounds after imposing the cuts of eqs.(21),(23), and the optimized cuts of eq.(25) (columns labeled as ‘OPT’). In the case  $M_{G^*} = 1.5 \text{ TeV}$  and  $2 \text{ TeV}$  the columns labeled as ‘OPT(II)’ report the value of the cross section after the alternative set of optimized cuts of eq.(26), in addition to those of eqs.(21),(23). For each channel, the proper branching fraction to a one-lepton final state has been included. Details on how the statistical errors and upper limits on the cross sections have been computed and combined are given in Appendix B.

LHC 14 TeV	$M_{G^*} = 1.5 \text{ TeV}$		$M_{G^*} = 2.0 \text{ TeV}$		$M_{G^*} = 3.0 \text{ TeV}$	$M_{G^*} = 4.0 \text{ TeV}$
	OPT	OPT(II)	OPT	OPT(II)	OPT	OPT
$G^* \rightarrow \tilde{T}t + Bb$	175.7(8)	133.0(7)	39.5(2)	32.3(2)	2.76(1)	0.231(1)
$WWbb$	3.9(3)	0.9(2)	1.0(2)	0.13(7)	0.02(5)	< 0.04
$Wbbj$	2.8(1)	1.34(8)	0.76(6)	0.37(4)	0.06(2)	0.005(7)
$Wbbjj$	1.20(4)	0.59(3)	0.32(2)	0.16(1)	0.028(6)	0.002(2)
$Wbbjjj$	0.10(1)	0.037(8)	0.022(6)	0.012(5)	< 0.002	< 0.002
$W3j$	0.60(2)	0.26(1)	0.21(1)	0.095(8)	0.043(5)	0.009(2)
$W4j$	0.28(2)	0.16(1)	0.10(1)	0.055(7)	0.025(5)	0.003(1)
Total background	8.9(3)	3.3(2)	2.4(2)	0.82(8)	0.18(5)	$(0.019^{+0.04}_{-0.007})$

Table 6: Cross sections, in fb, at  $\sqrt{s} = 14 \text{ TeV}$  for the signal and the main backgrounds after imposing the cuts of eqs.(21),(24), and the optimized cuts of eq.(25) (columns labeled as ‘OPT’). In the case  $M_{G^*} = 1.5 \text{ TeV}$  and  $2 \text{ TeV}$  the columns labeled as ‘OPT(II)’ report the value of the cross section after the alternative set of optimized cuts of eq.(26), in addition to those of eqs.(21),(24). For each channel, the proper branching fraction to a one-lepton final state has been included. Details on how the statistical errors and upper limits on the cross sections have been computed and combined are given in Appendix B.

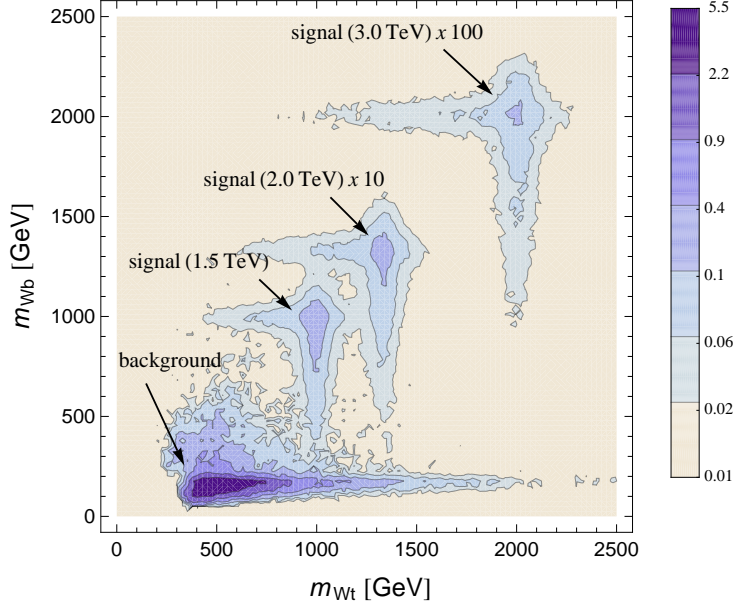


Figure 11: Contour plot of the signal and total background cross sections after the cuts at ‘zero cost’ of eq.(23) in the plane  $(m_{W_t}, m_{W_b})$ , where  $m_{W_b} \equiv m(W_{\cancel{t}}b_{\cancel{t}})$  and  $m_{W_t} \equiv m(W_{\cancel{t}}W_t b_{\cancel{t}})$ . The center-of-mass energy is  $\sqrt{s} = 7$  TeV. Different colors correspond to areas of different values of the doubly differential cross section  $d^2\sigma/dm_{W_b}dm_{tot}$ , as reported in the vertical color key on the right in units  $\text{ab}/\text{GeV}^2$ . The signals at  $M_{G^*} = 2.0$  TeV and 3.0 TeV have been rescaled respectively by a factor 10 and 100.

In the case of  $M_{G^*} = 1.5, 2.0$  TeV, we found that imposing cuts slightly stronger than those of eq.(25) can lead to a higher signal over background ratio,  $\mathcal{S}/\mathcal{B}$ , (although the corresponding discovery luminosity is also higher). Specifically, we find that the set of cuts that maximizes  $\mathcal{S}/\mathcal{B}$  is:

$$\begin{aligned}
 \underline{M_{G^*} = 1.5 \text{ TeV}} : \quad & m_{tot} \geq 1300 \text{ GeV} \quad m_{W_b} \geq 500 \text{ GeV} \quad m_{W_t} \geq 900 \text{ GeV} \\
 \underline{M_{G^*} = 2.0 \text{ TeV}} : \quad & m_{tot} \geq 1700 \text{ GeV} \quad m_{W_b} \geq 600 \text{ GeV} \quad m_{W_t} \geq 1100 \text{ GeV}.
 \end{aligned}
 \tag{26}$$

The values of the cross sections after imposing this alternative set of optimized cuts are reported in the columns of Tables 5 and 6 labeled as ‘OPT(II)’, respectively for  $\sqrt{s} = 7$  TeV and 14 TeV.

### 3.3 Discovery reach on the parameter space

All the numbers shown in Tables 5, 6 and 7 hold for the TS5 model at the benchmark point of eq.(18), where  $BR(G^* \rightarrow \tilde{T}t + Bb \rightarrow Wtb) = 0.25$  and the  $G^*$  production cross section is that of Fig. 1. It is however legitimate to ask how these results change when varying the model’s parameters. The production cross section scales with  $(\tan \theta_3)^2$ , while the branching ratio  $BR(G^* \rightarrow \tilde{T}t + Bb \rightarrow Wtb)$  is controlled by  $\tan \theta_3$ ,  $\sin \varphi_{tR}$ ,  $Y_*$  and the ratio of heavy



LHC $\sqrt{s} = 7$ TeV	$M_{G^*}$ [TeV]		
	1.5	2.0	3.0
$L_{disc}$ [fb $^{-1}$ ]	0.48	4.1	$1.3 \cdot 10^3$

LHC $\sqrt{s} = 14$ TeV	$M_{G^*}$ [TeV]			
	1.5	2.0	3.0	4.0
$L_{disc}$ [fb $^{-1}$ ]	0.054	0.24	3.4	57

Table 7: Value of the integrated luminosity required for a  $5\sigma$  discovery after the optimized cuts of eq.(25), for  $\sqrt{s} = 7$  TeV (upper panel) and  $\sqrt{s} = 14$  TeV (lower panel). The  $5\sigma$  discovery luminosity has been computed as explained in footnote 16.

masses  $M_{G^*}/m_{\tilde{T}}$ . To simplify the picture, we can fix the latter two parameters to the values adopted in the analysis,  $M_{G^*}/m_{\tilde{T}} = 1.5$  and  $Y_* = 3$ , and study the dependence on  $\tan\theta_3$  and  $\sin\varphi_{tR}$ . Figure 12 shows how the branching ratio varies in the plane  $(\sin\varphi_{tR}, \tan\theta_3)$ . It is possible to estimate how the LHC discovery reach varies with  $\tan\theta_3$  and  $\sin\varphi_{tR}$  by simply rescaling the numbers in Tables 5, 6 to take into account the change in the production cross section and in the branching ratio to the final state  $Wtb$ . The result is reported in Fig. 13. The two plots show the region in the plane  $(M_{G^*}, \tan\theta_3)$  where a  $5\sigma$  discovery is possible for the LHC at  $\sqrt{s} = 7$  TeV with  $L = 10$  fb $^{-1}$  (upper plot), and at  $\sqrt{s} = 14$  TeV with  $L = 100$  fb $^{-1}$  (lower plot). Three different degrees of compositeness of the right-handed top quark are considered:  $\sin\varphi_{tR} = 0.6, 0.8, 1$ . We expect that this simple rescaling reproduces reasonably well the actual reach one would obtain by optimizing the cuts at each different point of the parameter space. A possible bias can arise in the limit in which the decay width of the  $G^*$  or those of the heavy fermions become large, and tight cuts on the invariant masses have been applied. In this case, the efficiency of the kinematic cuts will in general depend non-trivially on the parameters via the particles' decay widths, and will not be reproduced by a simple rescaling. In our analysis the cuts on  $m_{Wb}$  and  $m_{Wt}$  are always much below the heavy fermions' masses, and also the cut on the total invariant mass should be sufficiently below the  $G^*$  mass to neglect, in first approximation, any deviation from the case of a simple rescaling.

The final results of our analysis, summarized by Tables 5, 6 and 7 and by the plots of Fig. 13, are very encouraging. For example, if  $\sin\varphi_{tR} = 0.6$  (a value which almost maximizes the branching ratio to  $Wtb$  in our model, see Fig. 12), the LHC at  $\sqrt{s} = 7$  TeV and with  $10$  fb $^{-1}$  of integrated luminosity should be able to discover a  $G^*$  with mass in the range  $M_{G^*} = (1.8 - 2.2)$  TeV for  $\tan\theta_3 = 0.2 - 0.5$ . On the other hand, by running at the design c.o.m. energy  $\sqrt{s} = 14$  TeV, the LHC discovery reach extends to the mass range  $M_{G^*} = (3.3 - 4.4)$  TeV for  $\tan\theta_3 = 0.2 - 0.5$  with an integrated luminosity  $L = 100$  fb $^{-1}$ .

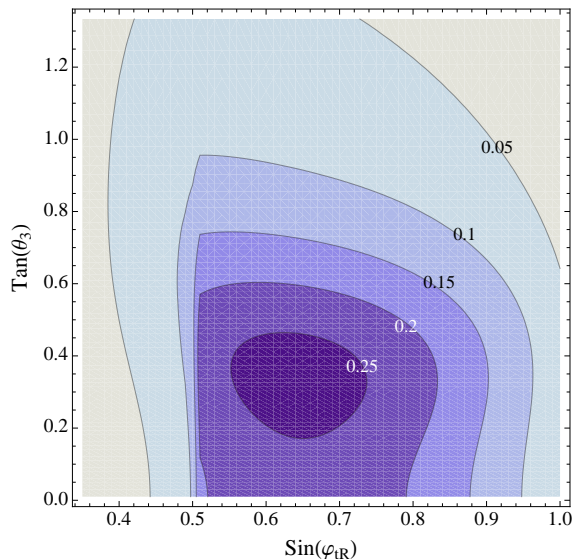


Figure 12: Isocurves of constant branching ratio  $BR(G^* \rightarrow \tilde{T}t + Bb \rightarrow Wtb)$  in the plane  $(\sin \varphi_{tR}, \tan \theta_3)$  with  $M_{G^*}/m_{\tilde{T}} = 1.5$  and  $Y_* = 3$ .

## 4 Discussion

In order to better quantify the potentiality of our analysis, it is useful to compare our results with those obtained in previous studies.

Ref. [5] searches for a KK-gluon in the channel  $G^* \rightarrow t\bar{t}$  and makes use of a LR polarization asymmetry to enhance the signal significance after cutting on the total invariant mass. The authors consider the case in which the right-handed top quark is fully composite, and adopt the following benchmark values of parameters:  $\tan \theta_3 = 0.2$ ,  $\sin \varphi_{tR} = 1$ ,  $\sin \varphi_L = 0.33$ ,  $Y_* = 3$ . The corresponding value of the couplings of  $G^*$  to the light quarks, top quark and bottom quarks is:  $g_{G^*q\bar{q}} = g_{G^*b_Rb_R} = -0.2 g_3$ ,  $g_{G^*t_Lt_L} = g_{G^*b_Lb_L} \simeq g_3$ ,  $g_{G^*t_Rt_R} = 5 g_3$ . The authors then assume that only decays of  $G^*$  to pairs of SM quarks are kinematically allowed, and obtain in this way a branching ratio  $BR(G^* \rightarrow t\bar{t}) \simeq 0.95$ . At the end of their analysis, they find  $\mathcal{S}/\mathcal{B} = 2$  (1.6) and  $\mathcal{S}/\sqrt{\mathcal{B}} = 11$  (4.2) for  $M_{G^*} = 3$  (4) TeV, where  $\mathcal{S}$  ( $\mathcal{B}$ ) is the number of signal (background) events expected at  $\sqrt{s} = 14$  TeV with an integrated luminosity  $L = 100 \text{ fb}^{-1}$ . These numbers are obtained without making use of the LR polarization asymmetry. This observable was proposed in Ref. [5] (see also Ref. [6]) as a way to better distinguish the signal from the background, but its quantitative impact on the signal significance was not derived by the authors. One way to compare with the above results is to consider the signal yield that we predict for  $\tan \theta_3 = 0.2$  and rescale it by a factor  $0.95/BR(G^* \rightarrow \tilde{T}t + Bb \rightarrow Wtb)$ , so that both results are normalized in the same way (*i.e.* to the same production cross section and decay branching ratio). In this way we obtain  $\mathcal{S}/\mathcal{B} = 9.3$  (3.0),  $\mathcal{S}/\sqrt{\mathcal{B}} = 44$  (7.3) for  $M_{G^*} = 3$  (4) TeV with  $L = 100 \text{ fb}^{-1}$  at  $\sqrt{s} = 14$  TeV.<sup>17</sup> This shows how powerful a search for  $G^* \rightarrow \tilde{T}t + Bb$  is, as a result of the strong reduction of

<sup>17</sup>In order to be conservative in our estimate, we have included a  $1\sigma$  upward fluctuation of the background from its central value quoted in Table 6.

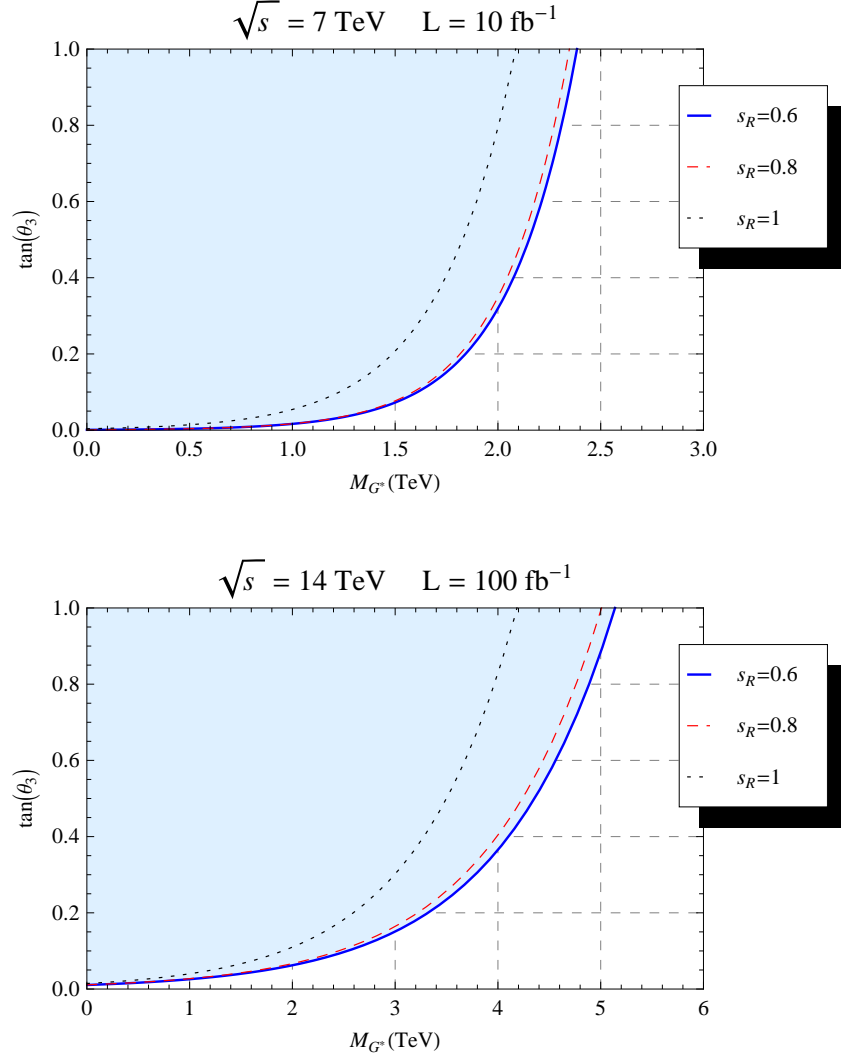


Figure 13: LHC discovery reach in the plane  $(M_{G^*}, \tan \theta_3)$ . The blue area shows the region where a discovery of the signal  $pp \rightarrow G^* \rightarrow \tilde{T}t + Bb \rightarrow Wtb$  is possible at  $5\sigma$  with  $\sin \varphi_{t_R} = 0.6$ ,  $M_{G^*}/m_{\tilde{T}} = 1.5$  and  $Y_* = 3$ . The reach at  $\sin \varphi_{t_R} = 0.8$  and  $\sin \varphi_{t_R} = 1$  is shown respectively by the dashed red curve and the dotted black curve. Upper plot: LHC at  $\sqrt{s} = 7 \text{ TeV}$  with an integrated luminosity  $L = 10 \text{ fb}^{-1}$ ; Lower plot: LHC at  $\sqrt{s} = 14 \text{ TeV}$  with  $L = 100 \text{ fb}^{-1}$ .

the SM background obtained by cutting on the invariant mass of the heavy fermion, compared to the ‘standard’  $t\bar{t}$  channel, although it must be noticed that the sensitivity of the latter is expected to increase when the information on the polarization of the  $t\bar{t}$  pair is included. Perhaps, a more sensible way to compare our results with those of Ref. [5] is by rescaling the  $t\bar{t}$  signal yield obtained in the latter to the branching ratio  $BR(G^* \rightarrow t\bar{t})$  predicted in our model at  $M_{G^*}/m_{\tilde{t}} = 1.5$ . For example we consider the benchmark values of the right plot of Fig. 4 ( $\tan \theta_3 = 0.2$ ,  $\sin \varphi_{tR} = 0.8$ ,  $\sin \varphi_L = 0.41$ ,  $Y_* = 3$ ), for which the branching ratios to  $Wtb$  and  $t\bar{t}$  are comparable:  $BR(G^* \rightarrow \tilde{T}t + Bb \rightarrow Wtb) = 0.21$ ,  $BR(G^* \rightarrow t\bar{t}) \simeq 0.41$ . After the appropriate rescaling, we find that with  $L = 100 \text{ fb}^{-1}$  at  $\sqrt{s} = 14 \text{ TeV}$  the analysis of Ref. [5] in this case predicts  $\mathcal{S}/\mathcal{B} = 0.86$  (0.69),  $\mathcal{S}/\sqrt{\mathcal{B}} = 4.7$  (1.8) for  $M_{G^*} = 3$  (4) TeV, while our result reads  $\mathcal{S}/\mathcal{B} = 2.0$  (0.66),  $\mathcal{S}/\sqrt{\mathcal{B}} = 9.7$  (1.6). On the other hand, in the extreme benchmark point of Ref. [5], where  $t_R$  is fully composite, we have checked that the  $t\bar{t}$  channel leads to a much better discovery reach than the one predicted by our analysis based on the  $Wtb$  channel. An opposite result is instead obtained for the benchmark values of eq.(18), for which the branching ratio to  $t\bar{t}$  is very small.

To summarize, we find that as long as the right-handed top quark is not exactly fully composite and the heavy gluon can decay to one or two heavy fermions, the branching ratio of the  $t\bar{t}$  channel decreases and the analyses based on it become less powerful. If decays to two heavy fermions are kinematically forbidden, on the other hand, a search based on the heavy-light decays to  $Wtb$  is very much competitive for the discovery of  $G^*$  and possibly stronger than the ‘standard’  $t\bar{t}$  searches. In addition, it gives the opportunity to discover both the heavy gluon and the new fermions at the same time. In fact, the process  $G^* \rightarrow \tilde{T}t + Bb$  turns out to be competitive for the discovery of the  $\tilde{T}$  and  $B$  as well.

It is useful, for example, to compare with the results obtained in Ref. [31], where the QCD pair production and the EW single production of the heavy bottom  $B$  were studied. At the end of their analysis, the authors find  $\mathcal{S}/\mathcal{B} = 1.45$  and a discovery luminosity  $L_{disc} = 4.3 \text{ fb}^{-1}$  for  $M_B = 1 \text{ TeV}$  at  $\sqrt{s} = 14 \text{ TeV}$ . For the same value of the heavy bottom mass,  $M_B = 1 \text{ TeV}$ , assuming  $M_{G^*}/m_B = 1.5$ , our analysis leads to a much smaller discovery luminosity, thanks to the larger rate of production of the signal. Taking into account only the signal  $G^* \rightarrow Bb \rightarrow Wtb$  (*i.e.* rescaling the signal yields of Table 6 by a factor  $\sim 2/3$  to subtract the contribution from  $\tilde{T}$ , see eq.(20)), we find  $\mathcal{S}/\mathcal{B} = 5.1 - 30$  and a discovery luminosity  $L_{disc} = (0.63 - 0.068) \text{ fb}^{-1}$  if  $\tan \theta_3$  varies in the range  $0.2 - 0.5$ .<sup>18</sup> This shows that the heavy-light decays of  $G^*$  can be an important mechanism for the production of the top and bottom KKs which should be taken into account, together with pair production and EW single production, to optimize the experimental searches.

Besides representing an additional and powerful way to discover the heavy fermions, the analysis of the heavy-light decays of  $G^*$  also gives the opportunity to extract some important properties of the new fermionic sector. A thorough analysis of the various heavy-light channels such as the one sketched in section 2.2 can indeed shed light on the quantum numbers of the heavy fermions and allow a determination of their couplings through the measurement of the branching ratios of  $G^*$ . Finding a large coupling of the top partners to  $G^*$ , for example, may give a first indication of their composite nature.

---

<sup>18</sup>Notice that our estimate of the discovery luminosity is more conservative than the one performed in Ref. [31], which is based on  $\mathcal{S}/\sqrt{\mathcal{B}}$ . For example, using the signal and background cross sections reported in Table 5 of Ref. [31] for  $M_B = 1 \text{ TeV}$ , we estimate  $L_{disc} = 6.7 \text{ fb}^{-1}$ , instead of  $4.3 \text{ fb}^{-1}$ .

So far, the experimental searches for new heavy fermions have mostly concentrated on their QCD pair production. This is expected to be the main production mechanism in the case of a fourth generation of chiral fermions, but it does not necessarily represent the best discovery process in the case of new vector-like fermions. At the same time, the experimental searches for a new heavy gluon have been so far performed only in the dijet and  $t\bar{t}$  channels. Our study shows that the presence of new heavy fermions has a strong impact on the phenomenology of the heavy gluon, and opens up new possibilities of discovery via its decays to one SM and one heavy fermion. The  $t\bar{t}$  experimental searches that are based on a full reconstruction of a pair of top quarks are in fact blind to these new processes. On the other hand, searches where the top quarks are not reconstructed, like for example those of Refs. [15–17], are sensitive to our signal  $G^* \rightarrow \tilde{T}t + Bb \rightarrow Wtb$ , but they are clearly less powerful than an optimized analysis, like the one proposed in this work, which exploits the peculiar kinematics of the signal. Optimizing the future experimental analyses to take into account the heavy-light decay topologies studied in this paper will give the opportunity to better explore the parameter space of theories beyond the Standard Model and possibly lead to the discovery of the sector responsible for the breaking of the electroweak symmetry.

## Note Added

While completing our work we became aware of the analysis of Ref. [62], where the heavy-light decays of a KK gluon are also studied. The importance of these latter to explain the forward-backward top quark asymmetry at the Tevatron was originally discussed in Ref. [63], as it was pointed out to us by J. Santiago.

## Acknowledgments

We thank B. Mele for participation in the early stages of this work and K. Agashe, G. Panico, A. Wulzer for discussions and comments. The work of R.C. was partly supported by the ERC Advanced Grant No. 267985 *Electroweak Symmetry Breaking, Flavour and Dark Matter: One Solution for Three Mysteries (DaMeSyFla)*. The work of N.V. was supported in part by DOE under contract number DE-FG02-01ER41155.

## Appendix

### A Lagrangian in the diagonal basis before EWSB

We collect here a few results on the TS5 model used in section 2. As explained in the text, the TS5 lagrangian (3) can be diagonalized, before EWSB, by performing a field rotation from the composite/elementary to the mass-eigenstate basis. More details on such rotation

will be given in a forthcoming publication [56]. The diagonalized lagrangian reads

$$\mathcal{L} = \mathcal{L}_{gauge} + \mathcal{L}_{fermion} + \mathcal{L}_{Higgs} \quad (27)$$

$$\begin{aligned} \mathcal{L}_{gauge} = & -\frac{1}{4}G_{\mu\nu}G^{\mu\nu} \\ & + \frac{1}{2}(D_\mu G_\nu^* D_\nu G_\mu^* - D_\mu G_\nu^* D_\mu G_\nu^*) + \frac{1}{2}M_{G^*}^2 G_\mu^{*2} + \frac{ig_3}{2}G_{\mu\nu}[G_\mu^*, G_\nu^*] \\ & + 2i g_3 \cot 2\theta_3 D_\mu G_\nu^* [G_\mu^*, G_\nu^*] + \frac{g_3^2}{4} \left( \frac{\sin^4 \theta_3}{\cos^2 \theta_3} + \frac{\cos^4 \theta_3}{\sin^2 \theta_3} \right) [G_\mu^*, G_\nu^*]^2 \end{aligned} \quad (28)$$

$$\begin{aligned} \mathcal{L}_{fermion} = & \bar{q} i \not{D} q + \bar{\psi} i \not{D} \psi + \bar{\chi} (i \not{D} - m_\chi) \chi \\ & - g_3 \tan \theta_3 G_\mu^* \bar{q} \gamma^\mu q + g_3 (\sin^2 \varphi_\psi \cot \theta_3 - \cos^2 \varphi_\psi \tan \theta_3) G_\mu^* \bar{\psi} \gamma^\mu \psi \\ & + g_3 \frac{\sin \varphi_\psi \cos \varphi_\psi}{\sin \theta_3 \cos \theta_3} G_\mu^* \bar{\chi} \gamma^\mu \psi + g_3 (\cos^2 \bar{\varphi}_\chi \cot \theta_3 - \sin^2 \bar{\varphi}_\chi \tan \theta_3) G_\mu^* \bar{\chi} \gamma^\mu \chi \\ & + h.c. + O(s_2) \end{aligned} \quad (29)$$

$$\begin{aligned} \mathcal{L}_{Higgs} = & |D_\mu H|^2 - V(H) \\ & + Y_* \cos \varphi_L \cos \varphi_{tR} \bar{Q}_L \tilde{H} \tilde{T}_R + Y_* \cos \varphi_{tR} \bar{Q}_{uL} H \tilde{T}_R - Y_* \sin \varphi_L \cos \varphi_{tR} \bar{q}_L \tilde{H} \tilde{T}_R \\ & - Y_* \sin \varphi_{tR} \bar{Q}_{uL} H t_R - Y_* \cos \varphi_L \sin \varphi_{tR} \bar{Q}_L \tilde{H} t_R + Y_* \sin \varphi_L \sin \varphi_{tR} \bar{q}_L \tilde{H} t_R \\ & - Y_* (s_2 \sin \varphi_L + s_3 \cos \varphi_L) \left( \cos \varphi_{tR} \bar{Q}'_L \tilde{H} \tilde{T}_R - \sin \varphi_{tR} \bar{Q}'_L \tilde{H} t_R \right) \\ & + Y_* \bar{Q}_R \tilde{H} \tilde{T}_L + Y_* \bar{Q}_u H \tilde{T}_L - s_4 Y_* \bar{Q}'_R \tilde{H} \tilde{T}_L \\ & + Y_* \cos \varphi_{bR} \bar{Q}_{dL} \tilde{H} \tilde{B}_R + Y_* \cos \varphi_{bR} \bar{Q}'_L H \tilde{B}_R - Y_* \sin \varphi_{bR} \bar{Q}_{dL} \tilde{H} b_R \\ & - Y_* \sin \varphi_{bR} \bar{Q}'_L H b_R - Y_* s_2 \cos \varphi_{bR} \bar{q}_L H \tilde{B}_R + Y_* s_2 \sin \varphi_{bR} \bar{q}_L H b_R \\ & - Y_* s_3 \sin \varphi_{bR} \bar{Q}_L H b_R + Y_* s_3 \cos \varphi_{bR} \bar{Q}_L H \tilde{B}_R \\ & + Y_* \bar{Q}'_R H \tilde{B}_L + Y_* \bar{Q}_{dR} \tilde{H} \tilde{B}_L + Y_* s_4 \bar{Q}_R H \tilde{B}_L + h.c. \end{aligned} \quad (30)$$

where  $q = u, d, c, s$ ,  $\psi = t_L, b_L, t_R, b_R$ , and we have defined  $Q = (T, B)$ ,  $Q' = (T', B')$ ,  $Q_u = (T_{5/3}, T_{2/3})$ ,  $Q_d = (B_{-1/3}, B_{-4/3})$ ,  $H = (\phi^+, \phi_0)$ ,  $\tilde{H} \equiv i\sigma^2 H^* = (\phi_0^\dagger, -\phi^-)$ .  $\chi$  denotes any of the heavy fermions, except in the first term in the third line of eq.(29), where it denotes a top or bottom heavy partner,  $T, B, \tilde{T}, \tilde{B}$ . Finally,  $s_3$  and  $s_4$  are defined as follows:

$$s_3 = \frac{\Delta_{L2} \bar{m}_{Q'}}{\Delta_{L1}^2 + \bar{m}_Q^2 - \bar{m}_{Q'}^2} \sin \varphi_L, \quad s_4 = \frac{\Delta_{L2} \Delta_{L1}}{\Delta_{L1}^2 + \bar{m}_Q^2 - \bar{m}_{Q'}^2}. \quad (31)$$

The coupling of  $G^*$  to the fermions are thus the following (we neglect terms of  $O(s_2)$ ):

$$g_{G^*qq} = -g_3 \tan \theta_3, \quad q = u, d, c, s \quad (32)$$

$$g_{G^*\psi\psi} = g_3 (\sin^2 \varphi_\psi \cot \theta_3 - \cos^2 \varphi_\psi \tan \theta_3), \quad \psi = t_L, b_L, t_R, b_R \quad (33)$$

$$g_{G^*\chi\psi} = g_3 \frac{\sin \varphi_\psi \cos \varphi_\psi}{\sin \theta_3 \cos \theta_3}, \quad \chi\psi = Tt_L, Bb_L, \tilde{T}t_R, \tilde{B}b_R \quad (34)$$

$$g_{G^*\chi\chi} = g_3 (\cos^2 \bar{\varphi}_\chi \cot \theta_3 - \sin^2 \bar{\varphi}_\chi \tan \theta_3), \quad \chi = \text{any of the heavy fermions}, \quad (35)$$

where  $\sin \varphi_{tL} = \sin \varphi_{bL} \equiv \sin \varphi_L$ , and we have defined  $\sin \bar{\varphi}_{T_L} = \sin \bar{\varphi}_{B_L} \equiv \sin \varphi_L$ ,  $\sin \bar{\varphi}_{\tilde{T}_R} \equiv \sin \varphi_{tR}$ ,  $\sin \bar{\varphi}_{\tilde{B}_R} \equiv \sin \varphi_{bR}$ , and  $\sin \bar{\varphi}_\chi = 0$  for any other heavy fermion  $\chi$ . In particular, at the benchmark point of eq.(18) we have:  $g_{G^*qq} = -0.44 g_3$ ,  $g_{G^*t_R t_R} = 0.53 g_3$ ,  $g_{G^*t_L t_L} = g_{G^*b_L b_L} = g_{G^*b_R b_R} = 0.40 g_3$ . The decay rates of  $G^*$  to two fermions are:

$$\Gamma(G^* \rightarrow q\bar{q}) = \frac{\alpha_3}{6} M_{G^*} \tan^2 \theta_3, \quad (36)$$

$$\Gamma(G^* \rightarrow \psi\bar{\psi}) = \frac{\alpha_3}{12} M_{G^*} (\sin^2 \varphi_\psi \cot \theta_3 - \cos^2 \varphi_\psi \tan \theta_3)^2, \quad (37)$$

$$\Gamma(G^* \rightarrow \chi\bar{\psi} + \psi\bar{\chi}) = \frac{\alpha_3}{6} M_{G^*} \frac{\sin^2 \varphi_\psi \cos^2 \varphi_\psi}{\sin^2 \theta_3 \cos^2 \theta_3} \left(1 - \frac{m_\chi^2}{M_{G^*}^2}\right) \left(1 - \frac{1}{2} \frac{m_\chi^2}{M_{G^*}^2} - \frac{1}{2} \frac{m_\chi^4}{M_{G^*}^4}\right), \quad (38)$$

$$\begin{aligned} \Gamma(G^* \rightarrow \chi\bar{\chi}) &= \frac{\alpha_3}{12} M_{G^*} \left\{ \left[ (\cos^2 \bar{\varphi}_\chi \cot \theta_3 - \sin^2 \bar{\varphi}_\chi \tan \theta_3)^2 + \cot^2 \theta_3 \right] \left(1 - \frac{m_\chi^2}{M_{G^*}^2}\right) \right. \\ &\quad \left. + 6 (\cos^2 \bar{\varphi}_\chi \cot^2 \theta_3 - \sin^2 \bar{\varphi}_\chi) \frac{m_\chi^2}{M_{G^*}^2} \right\} \sqrt{1 - 4 \frac{m_\chi^2}{M_{G^*}^2}}. \end{aligned} \quad (39)$$

Eq.(36) reports the decay rate to a pair of each species of light fermions,  $q = u, d, c, s$ , and the contribution of both chiralities has been included. Similarly, eq.(39) reports the decay rate to a pair of any of the heavy fermions,  $\chi$ , and the contribution of both chiralities has been included. As above,  $\psi = t_L, b_L, t_R, b_R$  in eqs.(37),(38).

The heavy fermions mostly decay to one longitudinally-polarized vector boson or Higgs boson plus one top or bottom quark, due to their large Yukawa coupling. The decay rates

into the three possible channels are:

$$\Gamma(\chi \rightarrow W_L \psi) = \frac{\lambda_{W\chi}^2}{32\pi} M_\chi \left[ \left(1 + \frac{m_\psi^2 - M_W^2}{M_\chi^2}\right) \left(1 + \frac{m_\psi^2 + 2M_W^2}{M_\chi^2}\right) - 4 \frac{m_\psi^2}{M_\chi^2} \right] \times \sqrt{1 - 2 \frac{m_\psi^2 + M_W^2}{M_\chi^2} + \frac{(m_\psi^2 - M_W^2)^2}{M_\chi^4}} \quad (40)$$

$$\Gamma(\chi \rightarrow Z_L \psi) = \frac{\lambda_{Z\chi}^2}{64\pi} M_\chi \left[ \left(1 + \frac{m_\psi^2 - M_Z^2}{M_\chi^2}\right) \left(1 + \frac{m_\psi^2 + 2M_Z^2}{M_\chi^2}\right) - 4 \frac{m_\psi^2}{M_\chi^2} \right] \times \sqrt{1 - 2 \frac{m_\psi^2 + M_Z^2}{M_\chi^2} + \frac{(m_\psi^2 - M_Z^2)^2}{M_\chi^4}} \quad (41)$$

$$\Gamma(\chi \rightarrow h\psi) = \frac{\lambda_{h\chi}^2}{64\pi} M_\chi \left(1 + \frac{m_\psi^2}{M_\chi^2} - \frac{M_h^2}{M_\chi^2}\right) \sqrt{\left(1 - \frac{m_\psi^2}{M_\chi^2} + \frac{M_h^2}{M_\chi^2}\right)^2 - 4 \frac{M_h^4}{M_\chi^4}}. \quad (42)$$

At  $O(r)$ , by using the Equivalence Theorem [61], the couplings  $\lambda_{W\chi}$ ,  $\lambda_{Z\chi}$ ,  $\lambda_{h\chi}$  can be extracted from the coefficients of the Yukawa terms in the diagonalized lagrangian (27).<sup>19</sup> In the case of the top and bottom partners, one has:

$$\lambda_{WT} = 0, \quad \lambda_{ZT} = \lambda_{hT} = Y_* \cos \varphi_L \sin \varphi_{tR} \quad (43)$$

$$\lambda_{WB} = Y_* \cos \varphi_L \sin \varphi_{tR}, \quad \lambda_{ZB} = \lambda_{hB} = 0 \quad (44)$$

$$\lambda_{W\tilde{T}} = \lambda_{Z\tilde{T}} = \lambda_{h\tilde{T}} = Y_* \sin \varphi_L \cos \varphi_{tR}, \quad (45)$$

$$\lambda_{W\tilde{B}} \simeq Y_* s_2 \cos \varphi_{bR}, \quad \lambda_{Z\tilde{B}} = \lambda_{h\tilde{B}} \sim Y_* \sin \varphi_{bR} \cos \varphi_{bR} \times O(r). \quad (46)$$

Notice, in particular, that the decay of  $\tilde{B}$  to  $Wt$  is suppressed by a factor  $s_2$ , since it must proceed via the mixing of the elementary  $b_L$  to the composite  $B'$ . On the other hand,  $\tilde{B}$  can decay to  $Zb_R, hb_R$  at next-to-leading order in  $r$ . Since under our assumptions  $s_2/\sin \varphi_{bR} = s_2/\sin \varphi_L = m_b/m_t \ll r \lesssim 1$ , it follows  $BR(\tilde{B} \rightarrow Zb + hb) \gg BR(\tilde{B} \rightarrow Wt)$ . We thus neglect the decay  $\tilde{B} \rightarrow Wt$  in our analysis.

## B Statistical Errors

In this appendix we give some details on how the statistical errors that appear in Tables 5 and 6 are computed and combined.

Let  $\sigma = \lambda a$  be the cross section for a given process, where  $\lambda$  is the number of events and  $a$  is a proportionality factor with no uncertainty. Then, if a Montecarlo simulation of the process returns  $n$  events, the true value  $\lambda$  is estimated following a Bayesian approach with

<sup>19</sup>See for example the discussion in footnote 2 of Ref. [27].



flat prior and posterior Poisson probability  $p(\lambda|n) = \lambda^n \exp(-\lambda)/n!$ . The latter has mean  $E[\lambda] = n + 1$  and variance  $V[\lambda] = n + 1$ , which implies a standard deviation on the cross section  $\delta\sigma = \sigma/\sqrt{n+1}$ . All the statistical errors on individual cross sections appearing in Tables 5 and 6 have been computed according to this formula.

In the case in which a set of kinematic cuts is applied to a sample of  $n_0$  simulated events with initial cross section  $\sigma_0$ , and no event passes the cuts, an upper bound on the final cross section can be derived at a given confidence level  $\alpha$  as the value  $\lambda_*$  for which

$$\int_0^{\lambda_*} d\lambda p(\lambda|0) = \alpha.$$

It thus follows  $\lambda_* = -\log(1 - \alpha)$ , which implies an upper limit on the final cross section  $\sigma < 1.1/(n_0 + 1)\sigma_0$  at 68% CL. All the upper limits that appear in Tables 5 and 6 are computed according to this formula and are at 68% CL.

When summing over the cross section of several processes, the statistical errors are combined in quadrature:

$$\delta\sigma_{tot} = \sqrt{\sum_i (\delta\sigma_i)^2}.$$

In the case in which on one of the initial cross sections there is an upper bound,  $\sigma_j < \bar{\sigma}_j$  at 68% CL, an asymmetric error on the total cross section is derived as follows:

$$\delta\sigma_{tot}^+ = \sqrt{\sum_{i \neq j} (\delta\sigma_i)^2 + \bar{\sigma}_j^2}, \quad \delta\sigma_{tot}^- = \sqrt{\sum_{i \neq j} (\delta\sigma_i)^2}.$$

The above definition is straightforwardly extended to the case in which more than one of the initial cross sections have an upper bound.

## References

- [1] L. Randall, R. Sundrum, Phys. Rev. Lett. **83** (1999) 3370-3373. [hep-ph/9905221].
- [2] H. Davoudiasl, J. L. Hewett, T. G. Rizzo, Phys. Lett. **B473** (2000) 43-49. [hep-ph/9911262]; A. Pomarol, Phys. Lett. **B486** (2000) 153-157. [hep-ph/9911294].
- [3] Y. Grossman, M. Neubert, Phys. Lett. **B474** (2000) 361-371. [hep-ph/9912408].
- [4] T. Gherghetta, A. Pomarol, Nucl. Phys. **B586** (2000) 141-162. [hep-ph/0003129].
- [5] K. Agashe, A. Belyaev, T. Krupovnickas, G. Perez and J. Virzi, Phys. Rev. D **77** (2008) 015003 [arXiv:hep-ph/0612015].
- [6] B. Lillie, L. Randall, L. -T. Wang, JHEP **0709** (2007) 074. [hep-ph/0701166].
- [7] B. Lillie, J. Shu, T. M. P. Tait, Phys. Rev. **D76** (2007) 115016. [arXiv:0706.3960 [hep-ph]].

- [8] A. Djouadi, G. Moreau, R. K. Singh, Nucl. Phys. **B797** (2008) 1-26. [arXiv:0706.4191 [hep-ph]].
- [9] R. Frederix, F. Maltoni, JHEP **0901** (2009) 047. [arXiv:0712.2355 [hep-ph]].
- [10] M. Redi, A. Weiler, [arXiv:1106.6357 [hep-ph]].
- [11] S. J. Huber, Q. Shafi, Phys. Lett. **B498** (2001) 256-262. [hep-ph/0010195].
- [12] S. Chatrchyan *et al.* [ CMS Collaboration ], [arXiv:1107.4771 [hep-ex]].
- [13] G. Aad *et al.* [ ATLAS Collaboration ], [arXiv:1108.6311 [hep-ex]].
- [14] The CDF Collaboration, CDF Note 9164 (2008).
- [15] The D0 Collaboration, D0 Conference Note 5882-CONF (2009).
- [16] The ATLAS Collaboration, Conference Note ATLAS-CONF-2011-087 (2011).
- [17] The ATLAS Collaboration, Conference Note ATLAS-CONF-2011-123 (2011).
- [18] The CMS Collaboration, *CMS Physics Analysis Summary* CMS-PAS-EXO-11-055 (2011).
- [19] The CMS Collaboration, *CMS Physics Analysis Summary* CMS-PAS-EXO-11-006 (2011).
- [20] R. Contino, Y. Nomura, A. Pomarol, Nucl. Phys. **B671** (2003) 148-174. [hep-ph/0306259].
- [21] K. Agashe, R. Contino, A. Pomarol, Nucl. Phys. **B719** (2005) 165-187. [hep-ph/0412089].
- [22] M. Carena, A. D. Medina, B. Panes, N. R. Shah, C. E. M. Wagner, Phys. Rev. **D77** (2008) 076003. [arXiv:0712.0095 [hep-ph]].
- [23] B. A. Dobrescu, K. Kong, R. Mahbubani, JHEP **0906** (2009) 001. [arXiv:0902.0792 [hep-ph]].
- [24] N. Vignaroli, arXiv:1107.4558 [hep-ph].
- [25] J. A. Aguilar-Saavedra, Phys. Lett. **B625** (2005) 234-244. [hep-ph/0506187]; J. A. Aguilar-Saavedra, PoS **TOP2006** (2006) 003. [hep-ph/0603199].
- [26] W. Skiba, D. Tucker-Smith, Phys. Rev. **D75** (2007) 115010. [hep-ph/0701247].
- [27] R. Contino, G. Servant, JHEP **0806** (2008) 026. [arXiv:0801.1679 [hep-ph]].
- [28] J. A. Aguilar-Saavedra, JHEP **0911** (2009) 030. [arXiv:0907.3155 [hep-ph]].
- [29] G. Azuelos, K. Benslama, D. Costanzo, G. Couture, J. E. Garcia, I. Hinchliffe, N. Kanaya, M. Lechowski *et al.*, Eur. Phys. J. **C39S2** (2005) 13-24. [hep-ph/0402037].

- [30] A. Atre, M. Carena, T. Han, J. Santiago, Phys. Rev. **D79** (2009) 054018. [arXiv:0806.3966 [hep-ph]].
- [31] J. Mrazek, A. Wulzer, Phys. Rev. **D81** (2010) 075006. [arXiv:0909.3977 [hep-ph]].
- [32] A. Atre, G. Azuelos, M. Carena, T. Han, E. Ozcan, J. Santiago, G. Unel, JHEP **1108** (2011) 080. [arXiv:1102.1987 [hep-ph]].
- [33] B. A. Dobrescu, C. T. Hill, Phys. Rev. Lett. **81** (1998) 2634-2637. [hep-ph/9712319].
- [34] R. S. Chivukula, B. A. Dobrescu, H. Georgi, C. T. Hill, Phys. Rev. **D59** (1999) 075003. [hep-ph/9809470].
- [35] K. Agashe, A. Delgado, M. J. May, R. Sundrum, JHEP **0308** (2003) 050. [hep-ph/0308036].
- [36] R. Contino, T. Kramer, M. Son and R. Sundrum, JHEP **0705**, 074 (2007) [arXiv:hep-ph/0612180].
- [37] J. M. Maldacena, Adv. Theor. Math. Phys. **2**, 231 (1998) [Int. J. Theor. Phys. **38**, 1113 (1999)] [arXiv:hep-th/9711200]; S. S. Gubser, I. R. Klebanov and A. M. Polyakov, Phys. Lett. B **428**, 105 (1998) [arXiv:hep-th/9802109]; E. Witten, Adv. Theor. Math. Phys. **2**, 253 (1998) [arXiv:hep-th/9802150].
- [38] N. Arkani-Hamed, M. Porrati, L. Randall, JHEP **0108** (2001) 017. [hep-th/0012148]; R. Rattazzi, A. Zaffaroni, JHEP **0104** (2001) 021. [hep-th/0012248]; M. Perez-Victoria, JHEP **0105** (2001) 064. [hep-th/0105048]; R. Contino, A. Pomarol, JHEP **0411** (2004) 058. [hep-th/0406257].
- [39] D. B. Kaplan, Nucl. Phys. B **365** (1991) 259.
- [40] R. Contino, L. Da Rold and A. Pomarol, Phys. Rev. D **75**, 055014 (2007) [arXiv:hep-ph/0612048].
- [41] M. S. Carena, E. Ponton, J. Santiago and C. E. M. Wagner, Nucl. Phys. B **759** (2006) 202 [arXiv:hep-ph/0607106]; A. D. Medina, N. R. Shah and C. E. M. Wagner, Phys. Rev. D **76** (2007) 095010 [arXiv:0706.1281 [hep-ph]].
- [42] G. Panico, A. Wulzer, [arXiv:1106.2719 [hep-ph]].
- [43] S. De Curtis, M. Redi, A. Tesi, [arXiv:1110.1613 [hep-ph]].
- [44] S. J. Huber, Nucl. Phys. B **666**, 269 (2003) [arXiv:hep-ph/0303183].
- [45] K. Agashe, G. Perez, A. Soni, Phys. Rev. Lett. **93** (2004) 201804. [hep-ph/0406101]; Phys. Rev. D **71**, 016002 (2005) [arXiv:hep-ph/0408134].
- [46] C. Csaki, A. Falkowski and A. Weiler, JHEP **0809**, 008 (2008) [arXiv:0804.1954 [hep-ph]].

- [47] M. Blanke, A. J. Buras, B. Duling, S. Gori, A. Weiler, JHEP **0903** (2009) 001. [arXiv:0809.1073 [hep-ph]].
- [48] K. Agashe, A. Azatov, L. Zhu, Phys. Rev. **D79** (2009) 056006. [arXiv:0810.1016 [hep-ph]].
- [49] O. Gedalia, G. Isidori, G. Perez, Phys. Lett. **B682** (2009) 200-206. [arXiv:0905.3264 [hep-ph]].
- [50] A. L. Fitzpatrick, G. Perez, L. Randall, [arXiv:0710.1869 [hep-ph]].
- [51] J. Santiago, JHEP **0812** (2008) 046. [arXiv:0806.1230 [hep-ph]].
- [52] C. Csaki, A. Falkowski, A. Weiler, Phys. Rev. **D80** (2009) 016001. [arXiv:0806.3757 [hep-ph]].
- [53] C. Csaki, G. Perez, Z. 'e. Surujon, A. Weiler, Phys. Rev. **D81** (2010) 075025. [arXiv:0907.0474 [hep-ph]].
- [54] K. Agashe, R. Contino, L. Da Rold and A. Pomarol, Phys. Lett. B **641** (2006) 62 [arXiv:hep-ph/0605341].
- [55] J. Mrazek, A. Pomarol, R. Rattazzi, M. Redi, J. Serra and A. Wulzer, Nucl. Phys. B **853** (2011) 1 [arXiv:1105.5403 [hep-ph]].
- [56] R. Contino, N. Vignaroli, in preparation.
- [57] J. Alwall *et al.*, JHEP **0709** (2007) 028 [arXiv:0706.2334 [hep-ph]]; F. Maltoni and T. Stelzer, JHEP **0302** (2003) 027 [arXiv:hep-ph/0208156]; T. Stelzer and W. F. Long, Comput. Phys. Commun. **81** (1994) 357 [arXiv:hep-ph/9401258].
- [58] M. L. Mangano, M. Moretti, F. Piccinini, R. Pittau, A. D. Polosa, JHEP **0307** (2003) 001. [hep-ph/0206293].
- [59] G. Aad *et al.* [ ATLAS Collaboration ], JINST **3** (2008) S08003.
- [60] A. Abdesselam, E. B. Kuutmann, U. Bitenc, G. Brooijmans, J. Butterworth, P. Bruckman de Renstrom, D. Buarque Franzosi, R. Buckingham *et al.*, Eur. Phys. J. **C71** (2011) 1661. [arXiv:1012.5412 [hep-ph]].
- [61] J. M. Cornwall, D. N. Levin and G. Tiktopoulos, Phys. Rev. D **10**, 1145 (1974) [Erratum-ibid. D **11**, 972 (1975)]; C. E. Vayonakis, Lett. Nuovo Cim. **17**, 383 (1976); B. W. Lee, C. Quigg and H. B. Thacker, Phys. Rev. D **16**, 1519 (1977). M. S. Chanowitz and M. K. Gaillard, Nucl. Phys. B **261**, 379 (1985).
- [62] R. Barcelo, A. Carmona, M. Chala, M. Masip, J. Santiago, [arXiv:1110.5914 [hep-ph]].
- [63] R. Barcelo, A. Carmona, M. Masip, J. Santiago, [arXiv:1106.4054 [hep-ph]].